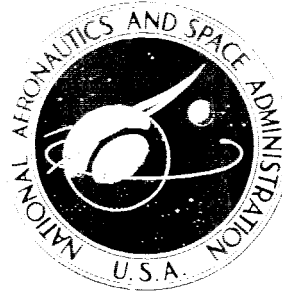


~~RESTRICTED DATA~~

~~CONFIDENTIAL~~

~~ATOMIC ENERGY ACT OF 1954~~

NASA TECHNICAL  
MEMORANDUM



UB

NASA TM X-2451

UB  
NASA TM X-2451

*[Faint, illegible text]*



*[Faint, illegible text]*

IN-PILE AND OUT-OF-PILE TESTING  
OF A MOLYBDENUM — URANIUM DIOXIDE  
CERMET FUELED THERMIONIC DIODE

*by Dominic C. DiIanni  
Lewis Research Center  
Cleveland, Ohio 44135*



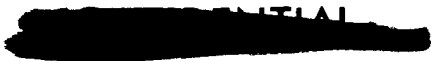
70580

1. Report No. TM X-2451		2. Government Accession No.		3. Recipient's Catalog No.	
4. Title and Subtitle <b>IN-PILE AND OUT-OF-PILE TESTING OF A MOLYBDENUM - URANIUM DIOXIDE CERMET FUELED THERMIONIC DIODE (U)</b>				5. Report Date January 1972	
				6. Performing Organization Code	
7. Author(s) Dominic C. DiIanni				8. Performing Organization Report No. E-5962	
9. Performing Organization Name and Address Lewis Research Center National Aeronautics and Space Administration Cleveland, Ohio 44135				10. Work Unit No. 112-27	
				11. Contract or Grant No.	
12. Sponsoring Agency Name and Address National Aeronautics and Space Administration Washington, D.C. 20546				13. Type of Report and Period Covered Technical Memorandum	
				14. Sponsoring Agency Code	
15. Supplementary Notes					
16. Abstract The purpose of this study was to determine the behavior of Mo-UO <sub>2</sub> cermet fuel in a diode for thermionic reactor application. The diode had a Mo-0.5 Ti emitter and niobium collector. Output power ranged from 1.4 to 2.8 W/cm <sup>2</sup> at emitter and collector temperatures of 1500° and 540° C. Thermionic performance was stable within the limits of the instrumentation sensitivity. Through 1000 hours of in-pile operation the emitter was dimensionally stable. However, some fission gases (15 percent) leaked through an inner clad imperfection that occurred during fuel fabrication. (U)					
17. Key Words (Suggested by Author(s)) Thermionic diode Inpile operation Mo-UO <sub>2</sub> fueled emitter Nb collector				18. Distribution Statement	
19. Security Classif. (of this report) Confidential		20. Security Classif. (of this page) Unclassified		21. No. of Pages 57	22. Price
GROUP 1 Excluded from automatic downgrading and declassification		<del>RESTRICTED DATA</del> 			

~~CONFIDENTIAL~~

~~CONFIDENTIAL~~  
CONTENTS

	Page
SUMMARY . . . . .	1
INTRODUCTION . . . . .	2
SYMBOLS . . . . .	3
EXPERIMENTAL PROGRAM AND TEST RESULTS . . . . .	4
Capsule Design and Fabrication (Ref. 5) . . . . .	4
Fuel form design . . . . .	4
Diode assembly . . . . .	5
Final assembly of capsule and out-of-pile and in-pile equipment . . . . .	6
Out-of-Pile Testing (Refs. 6 and 7) . . . . .	7
In-Pile Operation . . . . .	8
General operating conditions and history . . . . .	8
In-pile operating description . . . . .	9
In-pile operating history . . . . .	9
Operating data evaluation . . . . .	10
POSTIRRADIATION EXAMINATION OF CAPSULE AND FUELED EMITTER . . . . .	11
Capsule Support Hardware Examination . . . . .	11
Thermocouple failure . . . . .	11
Hermetic seal failure . . . . .	12
Internally finned sleeve failure . . . . .	12
Postirradiation Examination of Fueled Emitter . . . . .	13
Dimensional measurement . . . . .	14
Metallographic examination . . . . .	14
Burnup analysis . . . . .	15
Trapped fission gas analysis . . . . .	16
Fission products in neon volume . . . . .	17
CONCLUDING REMARKS . . . . .	18
Capsule Converter Performance . . . . .	18
Postirradiation Examination of Fueled Emitter . . . . .	19
APPENDIX - OUT-OF-PILE TESTING . . . . .	20
REFERENCES . . . . .	29



IN-PILE AND OUT-OF-PILE TESTING OF A MOLYBDENUM - URANIUM  
 DIOXIDE CERMET FUELED THERMIONIC DIODE (U)

by Dominic C. DiIanni  
 Lewis Research Center

SUMMARY

The purpose of this program was to determine the irradiation effects on the fuel emitter stability and the thermionic performance. The fueled emitter consisted of a molybdenum - uranium dioxide (Mo-UO<sub>2</sub>) cermet annulus clad both internally and externally with molybdenum - 0.5 titanium (Mo-0.5 Ti). The cermet fuel contained 58 weight percent UO<sub>2</sub> which was 40 percent enriched. The Mo-UO<sub>2</sub> cermet was fabricated from molybdenum-coated UO<sub>2</sub> spheroids having an average diameter of 300 microns. A finned niobium collector removed waste heat and was separated at temperature from the emitter by a 0.038-centimeter (0.015-in.) gap.

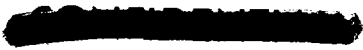
The diode was operated out-of-pile and then was tested in-pile under similar conditions. These conditions were the following:

Emitter temperature, °C . . . . .	1300 to 1500
Collector temperature, °C . . . . .	590 to 650
Output power, W . . . . .	31.9 to 63.8
Thermionic efficiency, percent . . . . .	4.2 to 6.7
In-pile operating period (output power > 1.4 W/cm <sup>2</sup> ), hr . . . . .	1040
In-pile operating period (output power = 2.8 W/cm <sup>2</sup> ), hr . . . . .	658
In-pile thermal cycles . . . . .	32

The diode operated 294 hours out-of-pile and had 19 thermal cycles.

The diode support hardware and instrumentation deteriorated after 1000 hours so it was impossible to continuously monitor diode performance. However, the diode was still operational at the end of irradiation.

The postirradiation examination showed the fuel burnup was  $6.5 \times 10^{19}$  fissions per cubic centimeter UO<sub>2</sub> (0.266 at.%). Diameter measurements of the emitter indicated no swelling occurred. Fifteen percent of the fission gases escaped through a flaw in the bond line formed by the inner clad and the bottom cap while 80 percent were retained in the UO<sub>2</sub> fuel particles. The bond of the outer clad to the fuel cermet was so good that it was difficult to follow at a  $\times 100$  magnification. Metallography showed the cermet remained intact and appeared to retain much of its strength while providing a path for fission gases to escape.



~~CONFIDENTIAL~~

## INTRODUCTION

The thermionic reactor offers the potential of achieving the compact, low specific weight power supply needed to meet future space power requirements. In the reactor many thermionic fuel elements are used to directly convert heat to electricity. In each fuel element are a number of unit cells or thermionic diodes which are electrically connected to provide the power output. Successful operation of a single, long life, reliable, thermionic diode is important in proving this direct conversion concept. Although diodes can be easily operated out-of-pile, the fundamental question in practical in-pile thermionics is the effect of the reactor environment on thermionic performance.

A key component of a thermionic diode is the fueled emitter which must operate at high temperatures with a high degree of dimensional stability. The amount of swelling establishes the useful life of a thermionic reactor. As little as 2 percent can limit reactor life to 10 000 hours (ref. 1). The main cause of swelling is fission gas pressure buildup and the low creep strength of clad materials at temperatures of interest. These can combine to give swelling rates too high for practical reactor lifetimes. The swelling problem has been attacked by strengthening (thickening) the clad, venting fission gases through the clad, or by strengthening the fuel phase through use of vented and nonvented molybdenum or tungsten cermets.

At Lewis Research Center, an effort is being placed on evaluating several fuel design concepts where the fission product gases are both vented (bulk  $\text{UO}_2$ , UC, and UC-ZrC) and nonvented (W- $\text{UO}_2$  and Mo- $\text{UO}_2$  cermets). Los Alamos has studied vented molybdenum - uranium dioxide (Mo- $\text{UO}_2$ ) cermet fuel forms (ref. 2). The present report treats a nonvented Mo- $\text{UO}_2$  concept which uses molybdenum-0.5 titanium (Mo-0.5 Ti) as the clad material. This fuel design concept minimizes the stress on the emitter clad by containing the fission gases within the crystal lattice of the  $\text{UO}_2$  particles in the cermet. There are values of  $\text{UO}_2$  particle size,  $\text{UO}_2$  operating temperature, and burnup which will result in containment of 90 percent of the fission gases (ref. 3). These values, which would predict a 10 000-hour reactor lifetime (ref. 4), were selected for this fuel emitter design. Specifically they are as follows:

- (1)  $\text{UO}_2$  particle diameter of 150 to 300 micrometers
- (2)  $\text{UO}_2$  operating temperature equal to or less than  $1600^\circ \text{C}$
- (3) Burnup of equal to or less than  $1\frac{1}{2}$  percent

The fuel emitter design was incorporated into an experimental diode and tested both in-pile and out-of-pile. The objectives of the testing were to

- (1) Evaluate the fueled emitter design after 1000 hours of irradiation with respect to dimensional stability and fission gas retention capability.
- (2) Demonstrate the reliability of this diode design in a nuclear environment.

████████████████████

(3) Compare thermionic performance between in-pile and out-of-pile operation for a period of 1000 hours.

This report describes the results of the diode thermionic performance, the fuel's ability to retain integrity, and the cladding's ability to contain fission gas without swelling. A description of the experiment facility is included. The emitter surface operated at  $1500^{\circ}\text{C}$  and the  $\text{UO}_2$  near  $1500^{\circ}\text{C}$  (and always  $<1600^{\circ}\text{C}$ ). The niobium collector was operated at  $500^{\circ}\text{C}$  ( $930^{\circ}\text{F}$ ). (All units appearing in parentheses were actual measured values.) An inner electrode gap of 0.38 millimeter (0.015 in. hot) permits significant emitter swelling without short circuiting. The thermionic power output ranged from 1.4 to 2.8 watts per square centimeter. However, most of the operating period was at 2.8 watts per square centimeters.

The Nuclear Division of Martin Marietta Corporation designed and fabricated the capsule and experimental systems and did the out-of-pile testing under NAS3-4727PB. Irradiation and postirradiation examination was done at the Plum Brook Reactor Facility (PBRF). Personnel responsible for the program were: E. Jules, Engineering Manger and J. D. Long, Project Engineer for Martin Marietta; and R. J. Galbo, Project Engineer at PBRF; D. E. Hegberg was NASA Project Manger for all phases up to the final portion of the postirradiation examination. The author assumed management at this point, directed the fuel investigation, and analyzed the data.

## SYMBOLS

A	Richardson constant, $120\text{ A/cm}^2\text{-K}$
A'	emitter surface area, $\text{cm}^2$
a/o	atom percent burnup based on total uranium atoms
$a_0, a_1$	constants
E	external voltage, V
e	electron charge, $1.6 \times 10^{-19}\text{ C}$
F	radiant interchange factor
I	output current, A
J	current density, $\text{A/cm}^2$
$K_M$	thermal conductivity of molybdenum, $\text{W/m-K}$
$K_{UM}$	thermal conductivity of Mo- $\text{UO}_2$ , $\text{W/m-K}$
k	Boltzmann constant, $1.381 \times 10^{-23}\text{ J/K}$

████████████████████

$P_{ax}$	axial heat loss, W
$P_e$	emitter input power at zero current, W
$P_{ec}$	electron cooling, W
$P_{ra}$	radial heat loss, W
$q'$	radial heat rate, W/m
$R_1$	emitter stem resistance, $\Omega$
$R_2$	tantalum load resistance, $\Omega$
$r_1$	inside radius of inner clad, m
$r_2$	outside radius of inner clad, m
$r_3$	inside radius of outer clad, m
$r_4$	outside radius of outer clad, m
$T$	temperature
$T_c$	collector temperature, $^{\circ}\text{C}$
$T_{es}$	emitter outer surface temperature, $^{\circ}\text{C}$
$T_{is}$	emitter inner surface temperature, $^{\circ}\text{C}$
$T_{sr}$	sight-ring temperature, $^{\circ}\text{C}$
$V$	diode voltage, V
$\epsilon_c$	emissivity of collector surface
$\epsilon_{es}$	emissivity of emitter surface
$\sigma$	Stefan-Boltzmann constant, $5.67 \times 10^{-8} \text{ W/m}^2\text{-K}^4$

## EXPERIMENTAL PROGRAM AND TEST RESULTS

### Capsule Design and Fabrication (Ref. 5)

Fuel form design. - The emitter fuel form is based on a conceptual reactor fuel element study conducted under NASA contract (ref. 1). This fuel element design provides a void inside the annular fuel form to collect fission gases in order to reduce the swelling rate during operation. In this experiment, however, the interior fuel surface was clad (see fig. 1) to prevent accidental vaporization of the fuel by the electron bombardment heater used during the out-of-pile testing. This inner clad represents a con-

[REDACTED]

servative deviation from the concept. The emitter should distort or swell at an accelerated rate since the interior void is not accessible for accumulating fission gases.

The fuel is a Mo-UO<sub>2</sub> cermet (average thickness, 2.288 mm (0.090 in.)) with 58 weight percent UO<sub>2</sub>, 40 percent enriched. The as-fabricated Mo-0.5 Ti outer clad thickness varied from 1.27 to 1.52 millimeters (0.050 to 0.060 in.). Figure 1 shows the overall dimensions of the emitter. The inside diameter is sufficiently large to permit the insertion of an electron bombardment heater (e. b. h.) for out-of-pile testing. Extending the interior clad of the emitter to form a long stem serves as the e. b. h. vacuum chamber.

Figure 2(a) shows an exploded view of the components of the fueled emitter as they are assembled for hot pressing. A Mo-UO<sub>2</sub> cermet fuel bushing was fabricated from molybdenum-coated UO<sub>2</sub> spheroids having an average diameter of 300 microns. The coated particles were cold compacted to form the bushing and then were sintered in argon at 1800° C. The bushing surfaces were coated with finely milled molybdenum powder to ensure a metallurgical bond between the fuel bushing and its adjacent components. Adjacent components consisted of the exterior sleeve, a center mandrel, and two end caps machined from bar stock of Mo-0.5 Ti. The exterior surfaces of these components were flame sprayed with zirconium oxide (ZrO<sub>2</sub>) to minimize molybdenum carbide (MoC) formation during hot pressing operations. The assembled fuel emitter was placed in graphite dies and hot pressed in the temperature range of 2060° to 2100° C and maximum pressure of  $3.449 \times 10^7$  newtons per square meter (5000 psi). A photomicrograph of the emitter cross section is shown in figure 2(b). Figure 2(c) shows a typical metallurgical bond between the fuel and cladding material.

After hot pressing the emitter was radially gammagraphed at 120° positions to inspect the bonding, fuel location, and general conformity to the dimensional requirements. The outside diameter was then reduced by centerless grinding which also removed the brittle surface layer of MoC formed during the hot pressing operation. The emitter surface was polished to a 16 rms finish using number 500 emery cloth. A blind hole was then bored into the center core of the fueled emitter to form an e. b. h. cavity leaving a 1.016-millimeter (0.040-in.) cladding on the inside diameter.

Diode assembly. - The components of the diode made of tantalum consist of the crimp tubing, the cesium reservoir, the cesium passage tube, and the electrical load. Niobium was used for the collector cap and the collector. The components were tungsten inert gas welded in a remotely operated chamber. Figure 3 shows the cross section of the assembled diode including the fueled emitter and stem assembly. The internal ceramic insulators were made of aluminum oxide (Al<sub>2</sub>O<sub>3</sub>).

Collector helical fins were mated with the fins of the internally finned sleeve as shown in figure 3. There was a 0.635-millimeter (0.025-in.) space between the mating

fins. This space containing neon gas was selected to give the proper heat transfer rate permitting the collector to operate at 538° C (1000° F). The thermal resistance could be changed to simulate the in-pile gamma heating effects by reducing the neon gas pressure to  $1.33 \times 10^4$  newtons per square meter (100 mm Hg) and below in this space during out-of-pile testing.

Final assembly of capsule and out-of-pile and in-pile equipment. - Figure 4 shows the diode assembly ready for encapsulation in a 2.44-meter- (96-in.-) long by 5-centimeter- (2-in.-) diameter cylindrical tube containing the necessary instrumentation. Diode instrumentation consisted of 12 thermocouples and 13 voltage probes. These thermocouples sensed temperature at the cesium reservoir (3), the collector (2), upper and lower shunt (2), the emitter (3), and the electrical load collar (2). Electrical leads were attached to the two cesium heaters, the upper shunt, the lower shunt, and the load collar.

This capsule was irradiated in the vertical tube (V-1) of the Plum Brook Reactor (PBR). Major support equipment necessary to operate the diode in the reactor, shown schematically in figure 5, consists of a vertical beam tube, a mechanism for positioning the capsule within the beam tube, and cooling systems.

A mechanical positioning device was designed for this experiment to vary the input power level of the capsule. Control of the input power was accomplished by varying the horizontal distance between the capsule and the reactor core. This positioning mechanism drove the capsule in a circular arc, the center was the centerline of the V-1 tube with the ends terminated on a V-1 diameter perpendicular to the adjacent core face. Based on the mockup reactor (MUR) experiments the diode neutron flux varied by a factor of 10 between these two extreme positions. Consequently, the diode input power could vary from approximately 140 to 1400 watts.

This experiment used the reactor primary cooling water system (PCWS) to remove the experiment waste heat. As shown in figure 5 the cooling water enters a hollow torque tube and flows down through the tube to a water box at the bottom of the V-1 tube. The principal exit from the water box is a 2.54-millimeter (0.10-in.) flow annulus formed by a concentric flow sleeve around the capsule. A second exit bypasses the capsule through an orifice in the top of the water box. During normal operation the thermal and hydraulic conditions were as follows:

Pressure, N/m <sup>2</sup> (psia) . . . . .	$7.58 \times 10^5$ (110, average)
Pressure drop across PCWS header, N/m <sup>2</sup> (psi) . . . . .	$3.79 \times 10^5$ (55)
Flow rate, m <sup>3</sup> /sec (gal/min) . . . . .	$1.14 \times 10^{-3}$ (18)
Inlet temperature, °C (°F) . . . . .	57 (135)
Outlet temperature, °C (°F) . . . . .	60 (140)

The flow sleeve is made of three tubular sections welded together. The upper and lower parts are stainless steel. The middle 15-centimeter (6-in.) section is also made of stainless steel and is surrounded with a thin (1.26-mm (0.050-in.)) sheet of NiVCo-10 (78 percent Co and 22 percent Ni). This portion of the flow sleeve depressed the flux in order to properly operate the diode (i. e. , 1500<sup>o</sup> C emitter temperature and 2 to 3 W/cm<sup>2</sup> diode output power and 1 kW input power) in the V-1 test hole. The thickness of the NiVCo sleeve was determined from tests in the MUR.

### Out-of-Pile Testing (Refs. 6 and 7)

The out-of-pile test fixture is shown schematically in figure 6. This fixture provides the necessary equipment to operate the diode in the same manner as in-pile. An e. b. h. installed in the emitter cavity simulated the in-pile heat source. Other equipment used in this set up consisted of a water cooling system, a neon pressurization system, and a vacuum system. Instrumentation leads normally used for in-pile operation were connected to a console similar to that existing for in-pile operation. This out-of-pile test fixture provided control on the coolant ( $7.89 \times 10^{-6}$  to  $3.15 \times 10^{-4}$  m<sup>3</sup>/sec (1/8 to 5 gal/min)), the cesium reservoir temperature (21<sup>o</sup> to 316<sup>o</sup> C (70<sup>o</sup> to 600<sup>o</sup> F)), the neon pressure ( $0.133$  to  $1.01 \times 10^5$  N/m<sup>2</sup> (0.001 to 760 mm Hg)), and the emitter temperature (to 1600<sup>o</sup> C).

The out-of-pile testing phase of this program consisted of first testing a prototype diode designated as TIE-I-P. From the test results of TIE-I-P, design changes were made and then three diode capsules were built. These capsules were designated as TIE-I-1, TIE-I-2, and TIE-I-3. The TIE-I-1 capsule did not perform as well as the prototype and consequently was used to check out the in-pile support hardware. The other two devices performed as well or better than the prototype during the out-of-pile testing programs. The TIE-I-2 was selected for the first irradiation and TIE-I-3 was considered the backup. The capsule was designed to operate at the following conditions:

Emitter temperature, <sup>o</sup> C . . . . .	1500
Collector temperature, <sup>o</sup> C ( <sup>o</sup> F) . . . . .	538 (1000)
Output power, W/cm <sup>2</sup> . . . . .	2 to 3
Input power, W . . . . .	1000
Efficiency, percent . . . . .	5 to 6

The prototype capsule demonstrated that more than 2 watts per square centimeter of output power could be achieved at the desired emitter temperature. The TIE-I-2 device performed slightly better than the prototype, and its operating characteristics were used to evaluate irradiation effects on thermionic performance.

████████████████████

These capsules had the following out-of-pile operating history:

	TIE-I-P	TIE-I-2	TIE-e
Normal operation, hr	1709	294	115
Thermal cycles	39	19	10
Neon volume outgassing, hr	139	99	170
Cesium volume outgassing, hr	85	225	165
Emitter at high temperature, hr	1933	618	450

The appendix describes the method of emitter temperature measurements, load optimization, shunt calibration, and diode performance.

### In-Pile Operation

General operating conditions and history. - The TIE-I-2 capsule ran initially as anticipated. Cesium vapor pressure was controlled at the reservoir. The gamma field was adequate to heat all other parts of the diode envelope to a higher temperature than the cesium reservoir. As power was applied to the cesium reservoir heaters the diode output current increased rapidly. The diode general operating conditions and history were as follows:

Emitter temperature, °C . . . . .	approximately 1300 to 1500
Collector temperature, °C (°F) . . . . .	590 to 650 (1090 to 1200)
Power output, W . . . . .	31.9 to 63.8
Power density, W/cm <sup>2</sup> . . . . .	1.4 to 2.8
Reactor angular position, deg . . . . .	77 to 103
Input power (fission + γ), W . . . . .	760 to 950
Thermionic efficiency, percent . . . . .	4.2 to 6.7
Reactor cycles . . . . .	9
Operating period (output power, ≥ 1.4 W/cm <sup>2</sup> ), hr . . . . .	1040
Operating period (output power = 2.8 W/cm <sup>2</sup> ), hr . . . . .	658
Number of thermal cycles . . . . .	32

(TIE-I-2 had undergone a total of 51 thermal cycles when out-of-pile operation is considered.) Various instrumentation failures occurred throughout the in-pile operating period. The test was terminated after 1000 hours when the diode could not be con-

~~CONFIDENTIAL~~

tinuously monitored. However, when the capsule was disassembled in the hot cell the experimental difficulties encountered during the irradiation could be explained.

In-pile operating description. - Input power to the capsule was controlled by varying the position of the capsule through a  $180^\circ$  arc inside the vertical test hole. In the  $0^\circ$  position, the capsule is farthest from the core in the horizontal plane, and the power level is the lowest. Normally, after the reactor was brought to full power, the capsule was rotated toward the core until the collector temperature rose to approximately  $387^\circ\text{C}$  ( $730^\circ\text{F}$ ). Then the cesium reservoir temperature was raised (above  $204^\circ\text{C}$  ( $400^\circ\text{F}$ ) by use of cesium reservoir heaters until the maximum output current was achieved. The capsule was then rotated further toward the core until the collector temperature increased approximately  $55.6^\circ\text{C}$  ( $100^\circ\text{F}$ ). The cesium temperature was reoptimized to give the maximum power output at the higher collector temperature. These steps were repeated until the collector temperature was raised to about  $601^\circ\text{C}$  ( $1117^\circ\text{F}$ ), a condition where the emitter temperature was estimated to be  $1500^\circ\text{C}$  (based on the out-of-pile test data) and the output power was above 2 watts per square centimeter. Table I illustrates a typical set of startup data.

In-pile operating history. - The TIE-I-2 capsule was installed on December 11, 1964, corresponding to reactor cycle 29P and ran until August 9, 1965, the end of the reactor cycle 37P. Postirradiation examination was conducted subsequently. Table II shows the operating history for this period including the thermal cycles.

During cycle 29P the experiment operated as anticipated. However, the collector temperatures were found to be  $60^\circ$  to  $80^\circ\text{C}$  ( $108^\circ$  to  $144^\circ\text{F}$ ) lower than similar out-of-pile data. The cesium reservoir temperature likewise was optimized at a  $34^\circ\text{C}$  ( $61^\circ\text{F}$ ) (approximately) lower temperature than when the diode operated out-of-pile. There was a large range in the temperature uncertainty on all thermocouples due to the uncertainty in the reference cold junction temperature as explained under Hermetic seal failure (p. 12). After 26 hours of steady-state operation one of the two collector thermocouples failed. The shutdown transients had no apparent effect on the diode operation. No degradation in diode output power was observed during the first cycle.

The experiment operated normally during cycle 30. There was no additional instrumentation failure during this period. Power mapping of the vertical tube to determine how gamma heating changed with angular travel was completed at the beginning of the cycle. Changes in gamma heating were then compared with the out-of-pile test data for different neon pressures. Since changes in gamma heating were negligible, there were no discernible trends in the data. Consequently, this test showed that the out-of-pile neon pressure equivalent for gamma heating would be in the range from  $4 \times 10^2$  to  $1.33 \times 10^4$  newtons per square meter (3 to 100 mm Hg).

The operation of the diode was normal up to the end of cycle 31, when the last collector thermocouple failed. During the remaining cycles (32 to 37P) the upper and

lower shunt temperatures were used to determine the collector temperatures. Figure 7 shows a relation between the collector temperature and the upper and lower shunt temperatures. During these last five cycles it was difficult to continuously measure output current. When the instrumentation did operate for short periods the data showed no change in diode performance.

The diode internal load calibration made during cycle 34P fell within the out-of-pile external and internal calibration curves (fig. 24, p. 54). During the last five cycles most of the diode operation continued at reduced power where the insertion angle was less than the angle where the output current begins to drop. A fuel surface temperature of  $1435^{\circ}\text{C}$  was achieved at a maximum output power of 2.8 watts per square centimeter. The fuel surface temperature ranged from  $1275^{\circ}$  to  $1435^{\circ}\text{C}$  during the periods of 1.4 watts per square centimeter operation. The experiment was terminated at the end of cycle 37P after 1040 hours of operation. Electrical tests at this point failed to determine whether the cause was internal or external to the diode.

Table III shows typical operating data for each reactor cycle when the output current was maximized. These conditions were, for many instances, maintained for only short intervals because of the erratic output signals. These signals at various times indicated that the emitter could be approaching an overheated condition. When this occurred the temperatures were lowered either automatically or manually. A typical set of out-of-pile data is given for comparison with the in-pile data. Although the data are not consistent, they do indicate the diode was operational at the time of removal. The data also indicate no gross deterioration in the thermionic performance over the in-pile operating period (specific power  $< 1.4\text{ W/cm}^2$ ).

Operating data evaluation. - Examination of the disassembled capsule revealed that the in-pile operating difficulties resulted from the capsule hardware failure and not the diode itself (as noted in the section Capsule Support Hardware Examination). With this knowledge, therefore, much of the operating data can be explained.

At the start of irradiation (up to cycle 32) the gross behavior of the experiment was quite good. However, because instrumentation failures occurred from cycle 32 on, it became difficult to determine if optimum conditions existed. Therefore, data shown in table III could not be accurately compared with each other or with the out-of-pile conditions. The data taken during this period (32 to 37P) showed that 670 hours of operation were accumulated at an output power of 1.4 watts per square centimeter or greater, and approximately 300 of those hours were at a power level of 2.8 watts per square centimeter. One should note that the output power density of 1.4 watts per square centimeter was below the design envelop of 2 to 3 watts per square centimeter.

In cycles 29 to 31, if one assumes a  $39^{\circ}\text{C}$  ( $70^{\circ}\text{F}$ ) temperature correction for the optimized cesium temperature of figure 8, the data then fall within the  $4 \times 10^2$  to  $1.33 \times 10^4$  newtons per square meter (3 to 100 mm Hg) out-of-pile neon pressure data of figure 20

████████████████████

(see p. 52). It is reasonable to assume this 39<sup>0</sup> C (70<sup>0</sup> F) compensation to allow for the excessively high temperature gradient across connector is due to gamma heat (discussed further in the Hermetic seal failure section). This comparison then shows that about 1.33×10<sup>4</sup> newtons per square meter (100 mm Hg) of neon pressure gives the equivalent effect of the gamma heating in the V-1 test hole.

The output current was determined from the lower shunt temperature, millivolts across the shunt, and the out-of-pile shunt calibration curve (fig. 24, p. 54). The shunt calibration curve was checked during in-pile operation (cycle 34P). This calibration was within the console calibrating current line and the external current line. Conservatively, the external current line was used to determine the values shown in table III.

Figure 9 is a correlation for determining in-pile emitter temperature from the output current and collector temperature. Figure 9 was generated from figures 17, 19, and 24 (see appendix). Only the data (fig. 19) that falls between the neon pressures of 4×10<sup>2</sup> and 1.33×10<sup>4</sup> newtons per square meter (3 to 100 mm Hg) was used in figure 9 since the in-pile operating data falls within this band. The in-pile emitter surface and fuel temperatures shown in table III were taken from figure 9 using the maximum output current and collector temperature.

The values of shunt voltage drop and temperature measured in-pile were converted to output current through figure 24. This output current together with the measured in-pile collector temperatures were converted to an emitter sight-ring temperature by using figure 19. The sight-ring temperature was finally converted to emitter surface temperature using figure 17.

## POSTIRRADIATION EXAMINATION OF CAPSULE AND FUELED EMITTER

### Capsule Support Hardware Examination

The purpose for examining the capsule was to determine if the erratic in-pile operating data were due to the capsule support hardware or the diode. The major effort was devoted to examining the fueled emitter, a key component that must meet strenuous requirements.

After transferring the capsule to the hot cell it was carefully disassembled and the parts were examined. Results of this examination revealed the causes of the in-pile difficulties to be in three major areas all unrelated to the fueled emitter or the diode. These areas were the thermocouples, the hermetic seal, and the internally finned sleeve.

Thermocouple failure. - There were thermocouple failures independent of any problems in the connector area of the hermetic seal. The Chromel leg of some of the

Chromel-Alumel thermocouples and the negative leg of some of the W-26Re - W-5Re thermocouples opened circuit while the other leg remained good. Similar failures were experienced by Atomic International (ref. 8) who by metallographic examination found the fracture to be one leg near the hot junction. We assumed that tensile failure was due to the greater coefficient of expansion of the sheath and insulator material in this area. Since the prototype capsule ran out-of-pile for 1700 hours without experiencing similar failures, it appears that the addition of gamma heat to the thermocouples may have caused the failure.

Hermetic seal failure. - The hermetic seal consists of 37 pins where the voltage and the thermocouple leads from the diode terminate in the neon portion of the capsule. Female pins were soldered (lead-tin) to these leads. The female pins in turn were slipped over the male pins of the hermetic seal forming the electrical connection. The hermetic seal was located a few inches above the reactor core when the capsule was positioned in the V-1 tube. When this area of the capsule was disassembled we found flowed solder and some female pins annealed and loose. On one side of the connector, molten solder flowed across two pair of pins that served as connecting points for thermocouples. Areas of the hermetic seal must have operated at a temperature of at least 250° C (the melting point of solder), while other areas of the hermetic seal operated near the cooling water temperature of 58° C (136° F). This thermal gradient across the hermetic seal was due to the gamma heating in the locale. Therefore, the reason for the lower millivolt thermocouple output (such as those monitoring cesium reservoir temperature) was due to the thermocouples terminating at a seal where it was not in an isothermal condition. A linear thermal gradient was assumed and the junction temperature correction was calculated. When this correction was applied to in-pile temperatures the values agreed much better with the out-of-pile data.

Internally finned sleeve failure. - As discussed previously, from cycle 32 to the end of irradiation it became difficult to maintain the desired output current for a prolonged period. Further disassembly of the capsule provided the answer to this problem.

The internally finned sleeve is a stainless steel cylinder located between the collector and the external capsule wall. This sleeve was designed to give the proper thermal gradient from the collector to the outer can. Three legs 120° apart extending alongside the diode load served as a positioning device for this sleeve. Tabbed feet at the end of each leg are sprung into a groove in the external capsule wall. When this part of the capsule was disassembled, these legs of the internally finned sleeve were bent inwardly and were touching the load causing an electrical short. Originally these support legs of the internally finned sleeve were straight. The gamma heat from the diode load caused the legs to run several hundred degrees warmer than the capsule outer wall (except at the tabbed feet). The legs bent inward from thermal expansion because the legs were axially constrained at one end by the tabbed feet and at the other end by the tight fit of

CONFIDENTIAL

the sleeve in the capsule container. There was a  $1.27 \times 10^{-4}$  meter (0.005 in.) clearance between the container inside diameter and the outside diameter of the internally finned sleeve. Initially this bending was not sufficient for the legs to contact the load. It appeared that when the diode cooled during each thermal cycle, the diode assembly loosened and slipped downward because of the shortened bent legs. This action was repeated with each succeeding thermal cycle creating a ratcheting effect until the bent legs touched the diode load. When the grounded legs touched the load, the instrumentation output was erratic. The evidence for this explanation is shown by the photographs in figures 10 to 12; all the photographs were taken during the disassembly in the hot cell. Figure 10 shows the internally finned sleeve after removal from the capsule outer container. The tabbed feet were out of and below the groove indicating a further downward displacement of the diode. Figure 11 shows where one of the bent legs came in contact with the load. This is indicated by the accumulation of dirt on the inside surface of the bent leg and the spot on the load. Figure 12 shows the internally finned sleeve which was in contact with the outer stainless steel can. It also shows an elongated spot indicating relative motion downward with respect to the stainless steel can.

We conclude from this examination that the in-pile operating difficulties encountered were due to the capsule support hardware failure rather than the diode itself.

## Postirradiation Examination of Fueled Emitter

An emitter must be capable of operating at high temperature with a high degree of dimensional stability for the expected life of the reactor. In order to meet such conditions the fuel emitter should be capable of accommodating the generated fission gases. The pressure exerted on the clad because of fission gas buildup can be minimized by limiting the fission gas release from the  $\text{UO}_2$ . This is accomplished when the  $\text{UO}_2$  is operated below  $1600^\circ \text{C}$  and when the burnup does not exceed  $1\frac{1}{2}$  atomic percent (ref. 2). At this low temperature the release mechanism is diffusion controlled and the release rate is exponential with temperature and proportional to the surface to volume ratio of the  $\text{UO}_2$  particle. Hopefully, the large diameter spherical  $\text{UO}_2$  particles ( $300 \mu\text{m}$ ) used in this emitter should retain all but a few percent of the fission gases. The object of the post-irradiation examination therefore is to evaluate how well this fuel met these criteria after an in-pile operating period of 1000 hours (0.27 at. % burnup) and at a temperature of approximately  $1500^\circ \text{C}$ . The fueled emitter contains an inner clad which prevents fission gas from collecting in the central cavity. Because of this design feature emitter swelling would occur at an accelerated rate. An actual reactor emitter would not contain such a barrier. Whether the fission gases leaving the fuel particle will diffuse to

the central void without cermet swelling is considered an open question. The postirradiation examination of the fueled emitter consisted of dimensional measurements, metallography, burnup analysis, and trapped fission gas analysis in the  $UO_2$  particle.

Fission gases were unexpectedly found in the neon volume during capsule disassembly. The problem of identifying the escape path of these fission gases led to performing various tests on the intact emitter to substantiate the gas source. These tests are briefly discussed at the end of this section.

Dimensional measurement. - The results of the emitter measurements are shown in table IV. The maximum diameter change that occurred over 1000 hours of operation was 0.20 percent at the bottom. We knew the emitter diameter did meet the tolerance specified on the design drawing. Therefore, the diameter change based on the minimum diameter gives the maximum possible growth that could have occurred during this period. It can be concluded that gross swelling did not occur.

Metallographic examination. - Items considered during the metallographic examination were as follows:

- (1) The condition of the clad
- (2) The condition of the bond between cladding pieces
- (3) The condition of the bond between the clad and the cermet fuel
- (4) The condition of the cermet matrix and the ability of the matrix to retain fission product gases
- (5) The condition of the  $UO_2$  and anything that may possibly affect the ability of the  $UO_2$  to retain the fission product gases
- (6) The location of the escape route of the fission gas found in the neon volume of the capsule

The clad surface examination revealed the surface was shiny with no degradation at a  $\times 30$  magnification. The sequence of cuts used in sectioning the emitter is shown in figure 13. One face of each cut was polished and examined at magnifications up to  $\times 100$ .

Figure 14 is a  $\times 50$  photomicrograph of a portion of the face examined for cut 4. It is typical of all portions at the clad, the cermet core and bond between the clad, and the core. The photomicrograph illustrates the following:

(1) The condition of the clad is excellent. The only detected changes in the clad were a small increase in the interstitial impurities (oxygen, nitrogen, or hydrogen). This is shown by the increase of precipitate phase and a large increase in the grain size. These large grains do not seem to have adversely affected the clad.

(2) The bond between the clad and the cermet matrix is also excellent. In no place was any separation evident; most of the bond line has been obliterated by interdiffusion and grain growth.

(3) The molybdenum matrix appeared to be in good condition and may have retained much of its original strength. The number of grains in the matrix has increased providing more grain boundary connections between  $\text{UO}_2$  particles. There is a possibility that these grain boundaries provide a path for the passage of fission gases between  $\text{UO}_2$  particles.

The  $\text{UO}_2$  particles appeared to have remained almost free of any cracks during irradiation. Many small spherical voids were formed typical of irradiated  $\text{UO}_2$ . The large dark areas are caused by "pull out" during metallographic preparation. Figure 15 is a  $\times 1000$  photomicrograph of a section through a  $\text{UO}_2$  particle. At  $\times 1000$  this figure shows a complete separation between  $\text{UO}_2$  and the molybdenum matrix achieving the "pea in a pod" concept. This could explain the lack of emitter swelling due to thermal cycling. However, it is an open question whether the "pea in a pod" condition would still prevail at a higher fuel burnup. This photomicrograph also shows that a second phase has formed in the  $\text{UO}_2$ . There is no evidence of what effect this second phase has on the ability of  $\text{UO}_2$  to retain fission product gases.

It was not until the face of cut 5 was examined that the path for the fission gas escape was located. This is shown in figure 16 which is a montage of photomicrographs ( $\times 100$ ) of a longitudinal section of the emitter (from the o.d. into the inner cavity) at the bond line between the side and end cladding pieces.

As can be seen, the bond between the end clad and the inner cavity clad is entirely different than the bond between the end clad and the outer cladding piece. The bond to the outer clad is so good that the bond line is difficult to follow (at  $\times 100$ ). This bond is typical of the bonds at the other (closed) end of the emitter for both the inner and outer clad. During fabrication, some of the cermet fuel got between the end cladding piece and the center cavity cladding so that in this area the cermet fuel extends through the cladding to the surface of the center cavity cladding. This seam of fuel cermet existed over  $180^\circ$  of the bonded area.

That these grains were effective in venting fission gases was shown by the following:

(1) Since no fission gases were detected in the cesium volume ( $< 3.33 \times 10^5$  disintegrations/sec ( $< 9.0 \mu\text{Ci}$ )) krypton-85 was found in the gas sample, all the gases that did escape from the emitter escaped through the cladding flaw to the inner cavity.

(2) As mentioned previously, considerable quantities of fission product gases were found in the neon volume (too much to have come only from the  $\text{UO}_2$  particles in the immediate area of the fuel imperfection).

(3) Thirty-five percent of the gases released from the  $\text{UO}_2$  particles escaped from the emitter.

Burnup analysis. - The burnup analysis was performed on two segments of the emitter designated as 8M and 10M. The technique used, a mass spectrometer determination, was based on the change in uranium-236 to uranium-235 ratio from pre- and

██████████

postirradiation determination. This method of analysis, commonly used at the Plum Brook reactor, is considered reliable. The results of this analysis are shown in table V.

The average thermal flux was calculated to be  $3.22 \times 10^{12}$  neutrons per second square centimeter when using the overall average burnup and time. This value compares very well with the thermal flux ( $3.512 \times 10^{12}$  neutrons/sec-cm<sup>2</sup>) determined from flux measurements made in the V-1 test hole in the mockup reactor (MUR). Total fission gases generated were calculated using the total production rate krypton and xenon (including iodine-135 xenon-135) obtained from reference 9 (38.53 total fission gas atoms/100 fissions). Therefore, the volume of gas generated using the overall average burnup of 0.266 atomic percent was calculated to be 1.76 cubic centimeters at standard temperatures and pressure (STP). The volumes so calculated for the maximum and minimum burnups (0.275 and 0.249 at. %) were 1.820 and 1.648 cubic centimeters at STP.

We can begin to evaluate how well the fission gases were retained by the clad and the amount held in the UO<sub>2</sub> particles. This evaluation can be based on information from the metallography examination, burnup analysis, and the trapped fission gas analysis discussed next.

Trapped fission gas analysis. - The purpose of this test is to determine the amount of fission gas trapped in the UO<sub>2</sub> particles, the clad, and the molybdenum matrix. Such information is valuable when determining pressure buildup on the clad due to the generated fission gases. Hopefully, fission gases trapped in the UO<sub>2</sub> particle contribute very little to pressure buildup as long as the UO<sub>2</sub> does not exceed a burnup of  $1\frac{1}{2}$  atomic percent and the operating temperature is less than 1600° C. Therefore, only the gases found in the matrix and clad and in the neon containment (0.2441 cm<sup>3</sup> STP) should be considered in any pressure buildup calculations for emitter swelling. It is this swelling rate that determines the thermionic reactor useful life. From the burnup analysis calculations the average total amount of fission gases generated at the end of irradiation was 1.76 cubic centimeters at STP, the mean value was 1.733 cubic centimeters. This analysis should show therefore that a large portion of gases should be trapped in the UO<sub>2</sub> particle.

The method used (described in ref. 10) consists of electrolytic dissolution of the clad matrix using NaOH and an acid (50 percent HNO<sub>3</sub> and 50 percent HCl) dissolution of the fuel. Greater than 99 percent of the krypton-85 fission gas collected in vials was gamma counted to determine the activity. The accuracy of this method for determining krypton-85 activity is  $\pm 2.5$  percent (standard deviation) at  $10^8$  disintegrations per minute. Table VI shows the data collected from separate selective dissolution of cladding and fuel from specimens 8M and 10M. The krypton-85 activity was used to calculate the volume of gas trapped in the clad and the interface region between the clad and the

[REDACTED]

matrix surrounding the fuel particle. None of the data in table VI were corrected for decay.

Table VII shows the calculated fission gas volumes from the previous data and the measured gas volumes from the initial capsule puncture, the emitter puncture, and the emitter leak test (discussed in the next section). The total fission gas generated (determined from the burnup analysis) was used as a basis for determining the percent release. The total trapped gases in molybdenum, clad, and  $\text{UO}_2$  plus the gas found in the neon volume did not agree with value determined from the burnup analysis. This was expected since some gas was lost during emitter sectioning. The molybdenum and  $\text{UO}_2$  proportions from the trapped gas analysis were applied to the total derived from the burnup analysis. This gave the reported fission gas distribution shown in table VII. These results are reasonable and do help to further explain results of the other phases of the postirradiation examination. The  $\text{UO}_2$  particles retained 80 percent of the fission gases. This value is considered low since we expected the  $\text{UO}_2$  to retain 90 percent of these gases (ref. 3). This point could have been more confidently evaluated if the fission gases were retained by the clad. However, it is also possible that the fuel had operated for short periods above  $1600^\circ\text{C}$  (since the fuel temperature was not accurately known), a temperature at which the fission gas release rate for  $\text{UO}_2$  increases.

Fission products in neon volume. - When the capsule was disassembled we found approximately  $1.05 \times 10^8$  disintegrations per second ( $2840 \mu\text{Ci}$ ) and  $7.7 \times 10^8$  disintegrations per second ( $20\ 840 \mu\text{Ci}$ ) of xenon-153 in the neon volume. The cesium gas containment was punctured and the gas was analyzed. The gas sample although of poor quality (contaminated with air during handling) contained  $< 3.33 \times 10^5$  disintegrations per second ( $< 9.0 \mu\text{Ci}$ ) of krypton-85 indicating the fission gases did not exist in this volume. Tests were run on the intact emitter to substantiate this gas source. These tests were as follows:

(1) Leak testing the intact emitter was performed in a vacuum chamber at  $260^\circ$  and  $538^\circ\text{C}$  ( $500^\circ$  and  $1000^\circ\text{F}$ ). Krypton-85 activity did exist in the gas sample taken during this test, which confirmed that fission gases found in the neon volume originated at the emitter.

(2) Emitter clad puncture and gas analysis were performed. The gas analysis showed only traces of fission gases. It was concluded that the fission gas which escaped the  $\text{UO}_2$  fuel particles was not held back by the clad (suggesting a leak).

When the capsule was examined it was concluded that the escape path from emitter cavity to neon containment was by means of the emitter thermocouples. (These thermocouples when proven unreliable during the out-of-pile test were cut off in the neon volume and the hot junctions remained in the emitter cavity.) In order to verify this escape path, pieces of emitter thermocouple wire were analyzed for fission product activity.

CONFIDENTIAL

The analysis consisted of leaching two short pieces (approx 2.5 cm) of thermocouple wire in concentrated nitric acid for 15 minutes. The position of these wires in the capsule assembly was unknown although they were taken from within the emitter stem. The leach solution was gamma scanned to determine relative levels of gamma emitters. Results tended to verify the conclusion that the emitter thermocouples constituted the escape path.

These tests showed the following:

- (1) Fission gases in the neon volume did originate from the emitter.
- (2) These gases were not present in the cesium envelope and therefore the diode performance was not affected by this leak.

## CONCLUDING REMARKS

### Capsule Converter Performance

Out-of-pile testing accomplished the objectives of demonstrating diode performance and debugging the capsule design. In retrospect the method used to determine emitter temperature is not considered accurate enough for fuel evaluation purposes. During out-of-pile testing an optical pyrometer was used to sight temperatures in the emitter cavity with a reproducible accuracy of  $\pm 25^{\circ}$  C. When applying the accuracy of this data to determine the in-pile emitter temperature the accuracy spread increased. This increased spread is the result of considering accuracies associated with the collector temperature, output power, and localized gamma heating as compared to neon pressure effects. For future in-pile testing the emitter temperature should be accurate to  $\pm 50^{\circ}$  C or better. This value was obtained from considering fission gas pressure buildup and clad stresses and creep rate to determine fuel swelling with burnup. It was concluded that in the future emitter thermocouples should be added as part of the capsule support hardware.

When the emitter temperature was at  $1500^{\circ}$  C the diode produced 2.8 watts per square centimeter for an in-pile period of 658 hours. During the remaining 382 hours the diode output power level ranged from 1.4 to 2.8 watts per square centimeter and thermionic efficiency ranged from 4.5 to 6.8 percent. Initially the diode performed as predicted. As the operation continued, monitoring became more difficult until at the end of 1040 hours it was impossible to continuously monitor the performance. When the capsule was disassembled, the cause for the erratic performance was determined to be in the capsule hardware and not the diode. Failures occurred at the hermetic seal, the instrumentation, and at the legs of the internally finned sleeve. The diode was still

CONFIDENTIAL

[REDACTED]

operative at the end of irradiation. The data showed no gross deterioration in thermionic performance within the limits of the instrumentation.

### Postirradiation Examination of Fueled Emitter

After 1000 hours of in-pile ( $6.5 \times 10^{19}$  fissions/cm<sup>3</sup> UO<sub>2</sub>) operation the bond between the clad and the cermet was in excellent condition. In all areas examined most bond lines were obliterated by interdiffusion and grain growth. The UO<sub>2</sub> particles appeared almost free of any cracks and many small spherical voids were formed, typical of irradiated UO<sub>2</sub>.

Fission gases amounting to 1.76 cubic centimeters at STP were calculated from the fuel burnup results ( $6.5 \times 10^{19}$  fissions/cm<sup>3</sup> UO<sub>2</sub>). Fourteen percent of this gas escaped through a bond defect between the inner clad and the end cladding piece (fig. 16). This defect occurred during fabrication when the cermet and clad end pieces were hot pressed. Dimensional measurements showed that fuel swelling did not occur. From the point of view of the experiment objectives the bond defect prevented an accelerated swelling rate. However, the 14 percent gas release through this defect showed that fission gases can permeate the cermet. The UO<sub>2</sub> particles retained 80 percent of the fission gases instead of the predicted 90 percent. These results showed the fuel cermet had not reached its limit of useful life as a thermionic emitter operating at 1500° C for a period of 1000 hours.

From this irradiation, the Mo-UO<sub>2</sub> fuel concept warrants further study to determine its limit of useful life. The capsule design should be modified for any future irradiations so that diode performance can be more accurately monitored. Furthermore, the capsule modification should include emitter thermocouples.

Lewis Research Center,

National Aeronautics and Space Administration,

Cleveland, Ohio, September 24, 1971,

112-27.

## APPENDIX - OUT-OF-PILE TESTING

This appendix covers a series of studies made during out-of-pile testing, and it contains the methods of measuring emitter temperatures, load optimization, shunt calibration, and diode performance.

### Emitter Surface Temperature Determination During Out-of-Pile Testing

This capsule and diode design offered no way of measuring the emitting surface temperature directly. A sight ring (shown in fig. 3) located on the inner wall of the emitter was used to determine the emitter temperature. The temperature measured at the sight ring was used to calculate the emitter surface temperature.

During the out-of-pile testing the temperature of a sight hole in the emitter sight ring was measured by an optical pyrometer. Measurements of the sight-hole temperature were difficult because of the long distance between the pyrometer and the target and, the small sight angles available. In addition, the blackbody hole geometry was not ideal for accurate measurements. At temperatures above  $1400^{\circ}\text{C}$  the contrast between the sight hole and the sight ring was sufficient so that the hole temperature had a reproducible reading accuracy of about  $\pm 25^{\circ}\text{C}$ . At temperatures of  $1300^{\circ}$  to  $1399^{\circ}\text{C}$  the reproducible accuracy was about  $\pm 40^{\circ}\text{C}$ . During out-of-pile testing the actual emitting surface temperatures were less than the inner surface measured by the pyrometer. The apparent sight-hole temperature was higher than the associated emitter inner wall temperature because of the reflected light from the heater filament and the radial heat flow across the sight ring. A special test was set up placing an emitter within a collector made up of three rings each about one-third as long as the emitter. Each collector ring was penetrated with a glass viewport through which the optical pyrometer could be sighted into a blackbody hole drilled into the emitter surface. The emitter was machined like the TIE-I emitter with one end closed and the other opened, but without the emitter stem. The special test setup had a plate similar to the TIE-I diode where the optical pyrometer could be sighted into the emitter cavity. The electron bombardment heater and the sight ring inside the emitter was also the same as the TIE-I diode.

The test procedure consisted of heating the emitter to the desired temperature until a steady-state condition was achieved. The heat transmitted to the collector was determined by measuring the temperature rise of the water cooling each collector ring. (The data consequence here involved only the middle ring since it was least affected by end losses.) The sight-ring and emitter surface temperatures were measured with the same optical pyrometer used for the TIE-I diode. This was repeated at various temperatures over the entire range of interest.

The emitter surface temperature data were corrected for the viewport glass effects. The sight-ring temperature did not require a correction since the same line-of-sight conditions existed in the TIE-I diode.

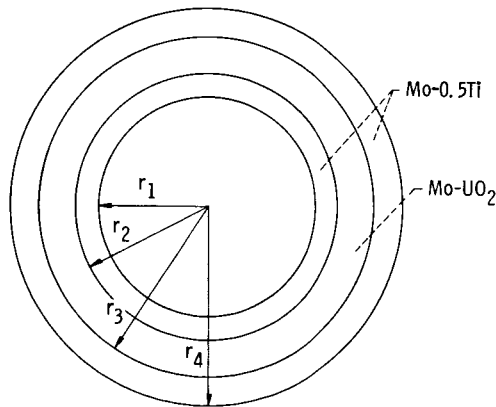
Data obtained during this study consisted of emitter outer surface temperature ( $T_{es}$ ), sight-ring temperature ( $T_s$ ), and radial heat rate ( $q'$ ). From these data the emitter inner surface temperature ( $T_{is}$ ) can be calculated.

The temperature drop through the emitter, due to thermal resistivity, was computed using the following equation, which assumes good thermal contact between the molybdenum clad and the cermet fuel:

$$T_{is} - T_{es} = \frac{q'}{2\pi} \left[ \frac{1}{K_M} \left( \ln \frac{r_2}{r_1} + \ln \frac{r_4}{r_3} \right) + \frac{1}{K_{UM}} \ln \frac{r_3}{r_2} \right]$$

where

- $K_M$  conductivity of molybdenum, 103.7 W/m-K (60 Btu/(ft)(hr)( $^{\circ}$ F))
- $K_{UM}$  conductivity of Mo-UO<sub>2</sub> cermet, 44.98 W/m-K (26 Btu/(ft)(hr)( $^{\circ}$ F))
- $r_1, \dots, r_4$  4.761 mm (0.188 in.), 5.78 mm (0.228 in.), 8.52 mm (0.335 in.), 9.53 mm (0.375 in.) emitter radii as noted in the sketch



The radial heat rate for the TIE-I emitter was based on 60 percent of the total emitter input power (for out-of-pile testing with output current). This reduction was determined from a digital computer program (ref. 11) and is treated in the section Out-of-Pile Diode Performance. The heat rate for the emitter in the test setup was taken as the heat transmitted through the middle collector ring.

Figure 17 shows the relation of the sight-ring temperature and the inner emitter

[REDACTED]

correlation test. A correction factor for the  $\Delta T$  across the sight ring to the inner emitter surface was determined. This was done by taking the  $\Delta T$  calculated for the emitter thickness alone and subtracting it from the  $\Delta T$  between the measured outer emitter surface and the sight ring. Then the TIE-I emitter surface temperature (during out-of-pile testing) was obtained by subtracting the correction factor and the calculated  $\Delta T$  across TIE-I emitter thickness from the sight-ring temperature. Shown in figure 17 are the corresponding emitter inner surface temperatures (applicable to the emitter in the test setup) and the fuel centerline temperatures as calculated from the previous equations. These curves show most of the difference between the sight-ring and emitting surface temperatures to be the experimental error between the sight-ring and the emitter inner surface temperatures. Thus, the fuel temperature should not be considered as the mean value between the sight-ring and the emitting surface temperatures.

### In-Pile Emitter Temperature Determination From Out-of-Pile Data

Examination of the TIE-I-P and TIE-I-2 data revealed a high degree of consistency when using the collector temperature as a measure of the power input to the emitter. This is illustrated in figure 18 for the TIE-I-2 capsule.

Emitter temperature is affected by both input and output power where the output power is a function of electron cooling. The relation of collector and emitter temperatures and output current at optimized cesium temperature is shown in figure 19. The collector temperature was raised by decreasing the neon pressure in the vacuum range, thereby increasing the heat resistance between collector surface and cooling water. Using collector temperature and optimized output current measured during in-pile operation, one may determine the emitter temperature by means of figure 19.

Effects of gamma heating were simulated during out-of-pile testing by varying the neon pressure between  $4 \times 10^2$  and  $1.01 \times 10^5$  newtons per square centimeter (3 and 750 mm Hg). In reference to figure 19 there was a slight change in output current (149 to 142 A) at the  $1500^\circ \text{C}$  emitter temperature line when the neon pressure was changed from  $4 \times 10^2$  to  $1.33 \times 10^4$  newtons per square meter (3 to 100 mm Hg). The collector temperature changed  $94^\circ \text{C}$  ( $170^\circ \text{F}$ ) over the same spread in neon pressure.

The emitter temperatures between  $1400^\circ$  and  $1740^\circ \text{C}$  were investigated for the TIE-I-2 by first establishing a neon pressure. And then, while holding a constant cesium temperature, the input power was varied. The constant cesium temperatures would generally fall between  $260^\circ$  and  $360^\circ \text{C}$  ( $500^\circ$  and  $680^\circ \text{F}$ ). To illustrate effects of the neon pressure change, figure 20 shows diode output current against cesium temperature and neon pressure as the parameter for a given collector temperature. Each curve

shows the rise and fall of emitter temperature. Note that the emitter temperature is near a minimum with maximum output current, a condition of maximum electron cooling.

### Load Optimization

Part of the diode design consisted of properly sizing the electrical tantalum load based on the operating characteristic of the diode. It was determined from a digital computer program that a tantalum tube with a 1.90-centimeter (0.75-in.) diameter, a 0.0305-centimeter (0.012-in.) thickness and a 8.26-centimeter (3.25-in.) length would be adequate. This phase of the out-of-pile testing using the TIE-I-P capsule checked this geometry.

Since this diode was fabricated with an integral load it was not possible to obtain variable load diode characteristics. However, data were obtained at different values of apparent load resistance by passing direct current through the load from an external source. Applying the current in the same direction as the diode output current effectively increased the load resistance, while applying the current in the opposite direction decreased it. Figure 21 shows an electrical diagram illustrating the external source hookup to the diode. Changing the load in this manner provided only a very small portion of the entire I-V curve, but it yielded information to determine the load characteristics at the desired diode operating range.

Three current-voltage curves are shown in figure 22 for conditions of optimum cesium temperature and emitting surface temperatures of 1425<sup>o</sup>, 1470<sup>o</sup>, and 1525<sup>o</sup> C. The dashed lines give the voltage across the tantalum load only. The highest current point on each dashed curve was obtained with no external current applied. Other points were obtained by increasing the load resistance with an external direct current. Added to each data point on the dashed curves was the voltage corresponding to the drop through the 1.0-milliohm resistance of the emitter stem.

The sensitivity of power output to the total load resistance can be seen to be quite small in figure 23. On the curve when emitting surface temperature is 1470<sup>o</sup> C, an increase in load resistance from 2.5 to 3.5 milliohms would drop output power to 2.95 watts per square centimeter. This drop in output power is 2 percent lower than the maximum condition (3.01 W/cm<sup>2</sup>). Likewise, the output power decreases to 2.83 watts per square centimeter going from the optimum at 2.5 to 1.5 milliohms. This is down to 6 percent from the maximum.

It was estimated that the higher load temperature resulting from gamma heating will increase the load from 2.85 to 3.25 milliohms. Since this represents a decrease in output on only 2 percent, no change in load geometry was recommended for TIE-I-2 capsule.

## Shunt and Load Calibration

At no time was it possible to measure output current directly. This section discusses the method used to determine the shunt and load calibration curve for computing output power. During diode operation the shunt temperature was measured for different voltage drops across the shunt and load. Then constructing a calibration curve of conductance (mho) against shunt temperature, the operating output current was computed. The previous calibration curve was used for the out-of-pile operation first and later verified for in-pile operations.

An accurate method of shunt calibration consists of passing a known direct current through the tantalum load. The calibrating current was measured with a 0.5-percent-accurate laboratory standard meter. The thermocouple output was read on the control console digital millivoltmeter.

During in-pile operation the shunt was calibrated by applying a current to the load from the power supply located in the control console. Figure 3 shows the voltage probe locations on the diode.

Figure 24 shows the data for shunt conductance against shunt temperature using both the external power supply and the control console power supply. The shunt conductance is shown to be essentially insensitive to change in neon pressure.

There were two distinct methods of applying calibrating current to the load, the console power supply, and an external supply. The conductance value when using the console calibrating power was higher. This might have been due to erroneously high temperature measurements due to local heating in the vicinity of the current carrying probe for the console-applied calibrating current. In this case, the temperature measurement would not be truly representative of the shunt temperature.

For all values of output current in this report, the conservative external calibrating curve was used.

Finally, the emitter stem resistance was calculated to be 0.0010 ohm, and this value was used for all stem voltage and diode power output results. The stem voltage drop was found to be between 35 and 41 percent of the total load voltage drop.

## Out-of-Pile Diode Performance

In order to evaluate the performance of TIE-I-diode both I-P and I-2 were operated to determine any performance degradation, electron cooling effects, and evaluation of the operating parameters.

The I-P diode operated consistently for 1709 hours. A comparison of the data showed no degradation in performance over this time period. The diode produced over

████████████████████

3 watts per square centimeter at a  $1505^{\circ}\text{C}$  emitting surface temperature ( $1625^{\circ}\text{C}$  sight-ring temperature) and a 6-percent device efficiency.

Comparing results of TIE-I-P and I-2 shows very good agreement. At  $1550^{\circ}\text{C}$  emitter temperature, I-P produced a maximum of 74 watts at a collector temperature of  $760^{\circ}\text{C}$  ( $1400^{\circ}\text{F}$ ), and I-2 produced a maximum of 70 watts at a collector temperature of  $704^{\circ}\text{C}$  ( $1300^{\circ}\text{F}$ ). The total load resistance was in both cases about 0.0028 ohm. The efficiency of I-2 is quite similar to I-P for nearly identical neon pressures. At about  $1.3 \times 10^2$  newtons per square meter (1 mm Hg), neon pressure I-P had an efficiency ranging from 5.7 percent at  $1500^{\circ}\text{C}$  to 6.1 percent at  $1700^{\circ}\text{C}$ . The efficiency of I-2 varied from 6.1 to 7.3 percent over the same emitter temperature range. In-pile performance of I-2 diode was compared with the I-P diode to determine gross (if any) irradiation effects on thermionic performance.

Since the out-of-pile results of I-P and I-2 were in good agreement, only the data of I-2 are presented. The data obtained were for various conditions of emitter, collector, and cesium temperatures at a maximum output current. The maximum output current conditions were obtained by varying the cesium temperature (cesium vapor pressure in inner electrode gap) while holding the emitter temperature constant. A wide range of neon pressures simulating gamma heating effects was investigated.

In figure 19 at an emitter temperature of  $1525^{\circ}\text{C}$  (the anticipated in-pile operating value) the output current shows a broad maximum with respect to changes in collector temperature. The collector temperature selected for in-pile operation ( $650^{\circ}\text{C}$  ( $1200^{\circ}\text{F}$ )) was at the low end of this range because it implies a safer emitter temperature in the event of an open circuit. Figure 25 is a plot of power input to the emitter against output power, with neon pressure as a parameter. It can be seen that a  $1.33 \times 10^{-1}$  newton per square meter (0.001 mm Hg) neon pressure between the collector fins results in an efficiency of less than 4 percent. For the neon pressure of about  $4 \times 10^2 \text{ N/m}^2$  (3 mm Hg), the diode operates at efficiencies between 7 and 8 percent.

The heat flow path from the emitter can be divided into two principal components: (1) heat that passes radially from the emitter to the collector by radiation, and (2) heat that leaves emitter in an axial direction. Performance data were used to determine how the heat flow changed with changes in output current. Data were taken at both the zero current condition and the typical operating condition. These determinations were then used to compare the design methods and assumptions used with the experimental observation.

Data listed in table VIII are experimental results with the exception of the emitting surface surface temperature. This value was obtained by applying the correction to the emitter sight-ring temperature shown in figure 17.

A least squares fit of the data (shown in table VIII) was performed in which the emitter input power, in the zero output current condition, was represented as

$$P_e = a_0 + a_1 T_{es} + \sigma FA' T_{es}^4 - T_c^4$$

where  $a_0 + a_1 T_{es} = P_{ax}$  is the heat loss axially, and  $\sigma FA' T_{es}^4 - T_c^4 = P_{ra}$  is the heat loss radially ( $T_{es}$  and  $T_c$  in K). In the axial heat loss equation,  $P_{ax}$  was assumed to be a linear function of the emitting surface temperature. The value of  $P_{ra}$  was determined and the data were then used to evaluate the other two constants,  $a_0$  and  $a_1$ .

With 0.25 for the emissivity of polished molybdenum at 1414° C (average emitting surface temperature for the 65 data points) and an assumed value of 1 for the niobium collector (observed to be dull gray after operating for about 200 hr), the radiant interchange factor was estimated as follows:

$$F = \left( \frac{1}{\epsilon_{es}} + \frac{1}{\epsilon_c} - 1 \right)^{-1} = 0.25$$

$$\epsilon_{es} = \text{emissivity of emitting surface} = 0.25$$

$$\sigma FA' = 32.3 \times 10^{-12} \text{ W/K}^4$$

This interchange factor was used to compute the quantity of radiant heat flowing from emitter to collector. When this heat rate was subtracted from the zero-current input power to obtain the axial heat loss, the latter was found to be the following linear function of emitter temperature:

$$P_{ax} = 0.992 T_{es} - 1280$$

Figure 26 shows most of the points to fall within a  $\pm 20$  percent error band. The average axial heat loss here is 60 percent.

The data in table VIII were expected to show that power input at constant emitter temperature would be a function of neon pressure. Since neon thermal conductivity across small gaps increases as gas pressure increases (from a vacuum to  $1.0 \times 10^5 \text{ N/m}^2$  (1 atm)), the heat loss from the emitter stem and collector end cap would be expected to increase. And since the emissivities of the emitter and collector surfaces change with time at high temperature, some change input power was also anticipated. However, no consistent trend with either variable was discernible from the out-of-pile

test data. Even though the data did not show a significant variation in the heat split with changes in neon pressure, the 40 to 60 percent heat split from the analysis is reasonable.

From the design (ref. 11) for the optimum output current conditions the heat split is reversed; that is, 60 percent is transferred to the collector and 40 percent is axially transferred through the stem and end cap. This is demonstrated by an analysis of the data shown in figures 27 and 28. From figure 27, at an emitting surface temperature of 1425° C, the power inputs for cesium temperatures of 221° C (431° F) (essentially zero output power) and 345° C (654° F) (maximum output current) are 665 and 1040 watts, respectively. Thus, the calculated heat split values for zero output current (40 to 60) and the output current case (60 to 40) are as follows:

	Zero output current, 665 W	Output current case (142 A), 1040 W
Axial heat rate, W	398	416
Radial heat rate, W	267	624

These data show that the axial heat rate remains essentially constant for both modes of operation, while a 357-watt increase occurred in the radial direction. This increase, primarily due to electron cooling, is substantiated when one considers the equation for calculating the electron cooling ( $P_{ec}$ ) in watts:

$$P_{ec} = \frac{IkT_{es}}{e} \left[ \ln \left( \frac{AT_{es}^2}{J} \right) + 2 \right]$$

where

e electronic charge,  $1.6 \times 10^{-19}$  C

k Boltzmann constant,  $1.38 \times 10^{-23}$  J/K

A  $120 \text{ A/cm}^2\text{-K}^2$

J output current per unit emitter surface area ( $I/22.8$ ),  $\text{A/cm}^2$

Now from figure 28, the corresponding output currents for an emitter temperature of 1425° C were 6 and 142 amperes, or 0.26 and 6.23 amperes per square centimeter.

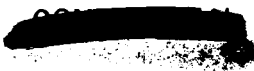
When this equation is applied to these data at 1425<sup>0</sup> C, the electron cooling for the low cesium temperature is

$$P_{ec} = 20.2 \text{ W}$$

and for high cesium temperature

$$P_{ec} = 412 \text{ W}$$

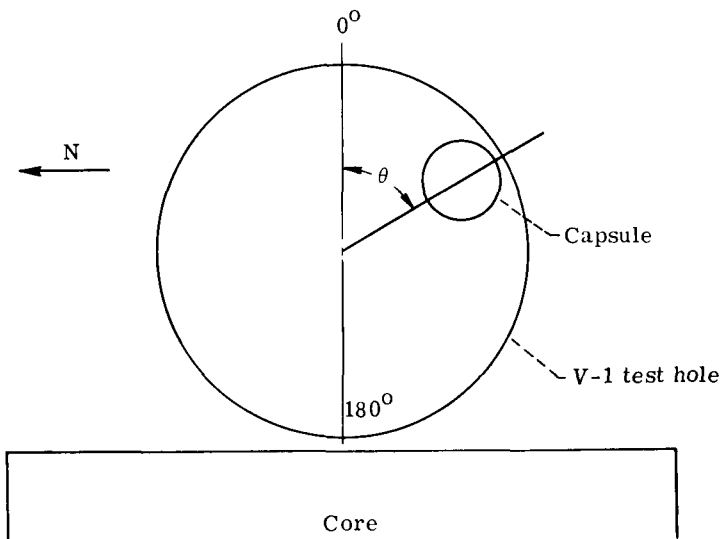
The difference is 392 watts (412 to 20.2) and agrees within 9 percent of the radial heat rate increase of 357 watts. From this type of analysis the 60-40 heat split appears to be reasonable.



## REFERENCES

1. Scicchitano, E. A. ; and Levedahl, W. J. : Analytical Study of In-Pile Thermionic Systems. Rep. MND-2997-1, Martin Co. (NASA CR-63134), 1963, Section 1.
2. Ranken, W. A. ; and Salmi, E. W. : Irradiation Studies of Mo 40 v/o UO<sub>2</sub> Cermet Fuel. Rep. LA-3237-MS, Los Alamos Scientific Lab. , June 16, 1965.
3. Reed, G. L. ; Scicchitano, E. A. ; and Levedahl, W. J. : Analytical Study of In-Pile Thermionic Systems. Rep. MND-2997-3, Martin Co. , 1963, p. II-5.
4. Scicchitano, E. A. ; and Levedahl, W. J. : Analytical Study of In-Pile Thermionic Systems. Rep. MND-2997-2, Martin Co. (NASA Cr-63488), 1963, pp. xii, I-8-I-10.
5. Stoffel, D. ; and Jules, E. : Design and Fabrication Report Encapsulated Thermionic Diode Thermionic Irradiation Experiment I (TIE-I). Rep. MND-3198, Martin Co. , Mar. 1965.
6. Long, J. D. ; and Frank, S. : Out-of-Pile Report TIE-I-P Performance Evaluation - Thermionic Irradiation Experiment I (TIE-I). Rep. MND-3161, Martin Co. , Sept. 1964.
7. Long, J. D. ; and Frank, S. : Out-of-Pile Test Report TIE-I-2 Performance Evaluation - Thermionic Irradiation Experiment I (TIE-I). Rep. MND-3162, Martin Co. , Oct. 1964.
8. Babbe, E. L. : Increasing Thermocouple Reliability for In-Pile Experiments. Rep. NAA-SR-10511, Atomics International, Apr. 20, 1965.
9. Anon. : Reactor Physics Constants. Rep. ANL-5800, Second ed. , Argonne National Lab. , July 1963, p. 8.
10. Sheibley, Dean W. : A Simple Method for Determination of Fission Gases Trapped in Irradiated Fuel Forms. NASA TM X-1893, 1969.
11. Bray, A. P. ; and MacCracken, S. J. : Tiger II - An IBM-704 Digital Computer Program: Temperatures from Internal Generation Rates. Rep. KAPL-2044, General Electric Co. , May 29, 1959.

TABLE I. - TYPICAL SET OF IN-PILE STARTUP DATA



Capsule position, $\theta$ , deg	Collector temperature		Cesium temperature		Load voltage, <sup>a</sup> V	Shunt voltage, V	Stem voltage, V	Output current, A	Output power, W
	$^{\circ}\text{C}$	( $^{\circ}\text{F}$ measured)	$^{\circ}\text{C}$	( $^{\circ}\text{F}$ measured)					
70.3	422	791	278	533	0.1638	0.0274	0.0969	96.9	25.25
80.7	483	901	276	528	.2175	.03705	.123	123	41.9
94	549	1020	288	550	.2585	.0445	.1399	139.9	55.8
103	603	1117	293	560	.2813	.0487	.1473	147.3	63.15

<sup>a</sup>All of the Ta load, including shunt.

TABLE II. - OPERATING HISTORY FOR TIE-I-2

Reactor cycle	Hours of operation with output power above $1.4 \text{ W/cm}^2$	Hours of operation at maximum output power of $2.8 \text{ W/cm}^2$	Thermal cycles
29P	147.1	137.1	2
30P	104.8	90.9	5
31P	115.8	104.2	2
32P	82.2	0	5
33P	175.9	0	3
34P	158.8	75.3	6
35P	185.6	181.5	1
36P	35.2	35.4	2
37P	35.0	35.0	6
Total in-pile	1040.4	659.4	32
Out-of-pile	294.0	294.0	19
Total	1334.4	953.4	51

**CONFIDENTIAL**

TABLE III. - TYPICAL IN-PILE OPERATING DATA COMPARED TO TYPICAL SET  
OF OUT-OF-PILE OPERATING DATA AT MAXIMUM OUTPUT CURRENT

Operating variables	Out-of-pile testing	In-pile testing								
		29	30	31	32	33	34	35	36	37
Cycle number	Out-of-pile	29	30	31	32	33	34	35	36	37
Reactor power, MW	-----	60	57	57	60	60	60	60	50	60
Position, deg	(a)	103	97	97.5	88	77	92.5	94	99	93
Output current, A	160	148	155.5	158	156	130	165	157.5	140	119
Collector temperature, °C (°F measured)	635 (1175)	605 (1122)	599 (1110)	608 (1127)	605 (1121)	481 (897)	563 (1045)	632 (1170)	574 (1065)	574 (1065)
Estimated emitter temperature, °C:										
Surface	1475	1420	1460	1470	1460	1345	1540	1470	1385	1250
Fuel	1510	1455	1495	1505	1495	1375	1580	1508	1415	1280
Optimum cesium temperature, °C (°F measured)	327 (620)	292 (558)	293 (559)	292 (558)	282 (540)	290 (555)	299 (570)	299 (570)	292 (558)	290 (555)
Shunt temperature, °C (°F measured)	-----	740 (1364)	731 (1349)	727 (1341)	679 (1255)	627 (1160)	693 (1280)	730 (1347)	668 (1235)	668 (1235)
Load voltage, V	0.285	0.281	0.290	0.292	0.269	0.2	0.27	0.282	0.233	0.212
Stem voltage, <sup>b</sup> V	0.160	0.148	0.155	0.158	0.156	0.130	0.165	0.158	0.140	0.119
Total voltage, V	0.445	0.429	0.445	0.450	0.425	0.340	0.437	0.440	0.373	0.331
Load resistance, Ω	0.00178	0.0019	0.00187	0.00185	0.00172	0.00161	0.00165	0.00179	0.00169	0.00179
Output power, W	71.2	63.5	69.1	71.0	66.4	44.1	72.2	69.3	52.2	39.5
Power density, W/cm <sup>2</sup>	3.12	2.79	3.03	3.11	2.91	1.94	3.17	3.04	2.29	1.74
Date (time of point)	-----	12/12/64 (0033)	2/27/65 (1130)	3/17/65 (0500)	4/6/65 (2180)	5/1/65 (0915)	5/21/65 (2250)	6/24/65 (0300)	7/17/65 (0100)	7/31/65 (0047)

<sup>a</sup>Neon pressure,  $1.33 \times 10^4$  N/m<sup>2</sup> (100 mm Hg).

<sup>b</sup>Current, 0.0010 A.

TABLE IV. - EMITTER DIMENSIONS BEFORE AND AFTER IRRADIATION

Location	Irradiated capsule diameter measurements			Before irradiation diameter, <sup>a</sup> cm (in.)	Increase	
	First value, cm (in.)	Second value (90 <sup>0</sup> rotation), cm (in.)	Average diameter, cm (in.)		cm (in.)	Percent
Top	1.9228 (0.7570)	1.9225 (0.7569)	1.9228 (0.7570)	1.920 (0.7560)	0.00259 (0.001)	0.13
Middle	1.9233 (.7572)	1.9220 (.7567)	1.9228 (.7570)	1.920 (.7560)	.00259 (.001)	.13
Bottom	1.9238 (.7574)	1.9241 (.7575)	1.9241 (.7575)	1.920 (.7560)	.003556 (.0015)	.20

<sup>a</sup>Values obtained from the design drawing having a tolerance of 1.9215 cm/1.920 cm (0.7565 in./0.7560 in.).

TABLE V. - BURNUP DETERMINATION ON FUEL SOLUTIONS OF EMITTER SECTIONS 8M AND 10M (SEE FIG. 13)

	Burnup determination of emitter sections 8M and 10M, at. % (fissions/cm <sup>3</sup> fuel UO <sub>2</sub> )	
Aliquot a	0.269 (6.60×10 <sup>19</sup> )	0.249 (6.11×10 <sup>19</sup> )
Aliquot b	.272 (6.66×10 <sup>19</sup> )	.275 (6.74×10 <sup>19</sup> )
Average	.270 (6.62×10 <sup>19</sup> )	.262 (6.40×10 <sup>19</sup> )
Overall average	0.266 (6.52×10 <sup>19</sup> )	

~~CONFIDENTIAL~~

TABLE VI. - FISSION PRODUCT DATA ON EMITTER

SECTIONS 8M AND 10M

[See fig. 13.]

	Emitter section	
	8M	10M
Weight of specimen, g	8.1078	9.2880
Weight of uranium includes uranium-235 + uranium-238 <sup>a</sup>	1.495	1.7412
Krypton-85 disintegrations/min from clad and matrix <sup>b</sup>	$1.25 \times 10^8$	$1.24 \times 10^8$
Krypton-85 disintegrations/min from fuel <sup>b</sup>	$1.52 \times 10^9$	$1.83 \times 10^9$
Ratio of Kr <sup>85</sup> fuel/Kr <sup>85</sup> clad	12.1	14.7

<sup>a</sup>These values were determined colorimetrically from acid dissolution of uranium dioxide only. The 8M cladding solution contained 24 mg uranium (as U<sup>238</sup>); 10M cladding solution contained 30.5 mg uranium (as U<sup>238</sup>).

<sup>b</sup>Data based on counted data 6/5/68 for cladding; 6/7/68 for fuel.

TABLE VII. - COMPLETE INVENTORY OF FISSION GASES

FOUND<sup>a</sup> IN CAPSULE AND FUELED EMITTER

[Fission gases considered were krypton-83, -84, -85, -86, xenon-131, -132, -133, -134, -135, and -136.]

Locations and methods	Mean
Gases found in the neon volume	0.2241
Gases found during puncture and emitter leak tests	.00025
Gases determined from burnup analysis	1.733
Gases found in uranium dioxide pellets	.879
Gases found in clad and matrix	.06545
Total gases calculated in uranium dioxide based on burnup analysis	1.385
Total gases escaped from the uranium dioxide particle	.348
Total gases held in matrix and clad	.104
Percent retained in uranium dioxide fuel part	79.9
Percent released from clad	14.1

<sup>a</sup>All values are cm<sup>3</sup> STP corrected to end of irradiation.

TABLE VIII. - OUT-OF-PILE TEST DATA AT  
ZERO OUTPUT CURRENT

Emitter power input, W	Emitter sight-ring temperature, °C	Emitting surface temperature, °C <sup>a</sup>	Neon pressure		Collector temperature	
			N/m <sup>2</sup>	mm Hg	°C	°F
738	1610	1490	4.6×10 <sup>2</sup>	3.5	602	1115
504	1460	1370	39	.3	472	881
645	1575	1465	↓	↓	604	1120
766	1675	1545	↓	↓	699	1290
872	1715	1575	↓	↓	766	1410
730	1615	1495	↓	↓	671	1240
670	1540	1436	↓	↓	644	1191
456	1380	1305	↓	↓	441	825
414	1315	1255	9.9×10 <sup>3</sup>	75	232	450
623	1520	1420	↓	↓	339	642
742	1620	1500	↓	↓	393	740
913	1695	1560	↓	↓	449	841
1030	1755	1610	↓	↓	499	930
1030	1750	1605	1.99×10 <sup>3</sup>	150	488	910
892	1675	1545	↓	↓	441	825
724	1550	1445	↓	↓	399	750
504	1385	1310	↓	↓	288	550
298	1185	1150	1.73×10 <sup>2</sup>	1.3	243	470
396	1305	1245	↓	↓	332	630
470	1400	1325	↓	↓	388	730
557	1500	1405	↓	↓	454	850
685	1605	1490	↓	↓	588	1090
857	1700	1565	↓	↓	666	1230
770	1640	1515	6.6	.05	729	1345
624	1545	1440	↓	↓	682	1260
448	1435	1350	↓	↓	548	1018
340	1310	1250	↓	↓	404	760

<sup>a</sup>Correlation of emitter sight-ring and emitting surface temperature from fig. A-1.

CONFIDENTIAL

TABLE VIII. - Continued. OUT-OF-PILE TEST DATA AT  
ZERO OUTPUT CURRENT

Emitter power input, W	Emitter sight-ring temperature, °C	Emitting surface temperature, <sup>a</sup> °C	Neon pressure		Collector temperature	
			N/m <sup>2</sup>	mm Hg	°C	°F
358	1270	1220	1.06×10 <sup>2</sup>	0.8	279	534
474	1375	1305	↓	↓	366	690
647	1500	1405	↓	↓	510	950
778	1600	1485	↓	↓	588	1090
971	1700	1565	↓	↓	691	1275
772	1665	1535	10.6	.08	714	1317
589	1525	1425	10.6	.08	599	1110
605	1525	1425	3.3×10 <sup>2</sup>	2.5	452	845
800	1660	1530	3.3	2.5	571	1060
610	1525	1425	3.3	2.5	449	840
621	1525	1425	1.46×10 <sup>3</sup>	11.0	393	740
777	1660	1530	1.46	11.0	466	870
776	1665	1535	10.6	.08	735	1355
571	1525	1425	10.6	.08	549	1020
589	1525	1425	6.6×10 <sup>2</sup>	5	416	780
829	1665	1535	6.6	5	535	995
843	1665	1535	5.3×10 <sup>3</sup>	40	452	845
636	1525	1425	5.3	40	371	700
797	1665	1535	2.93	220	396	745
657	1525	1425	2.93	220	346	655
313	1200	1160	26	.2	307	585
533	1370 to 1400	1310	↓	↓	516	960
675	1435 to 1445	1345	↓	↓	621	1150
773	1470	1380	↓	↓	702	1295
915	1600	1485	↓	↓	781	1438
937	1630	1510	↓	↓	816	1500
1051	1700	1565	↓	↓	868	1595

<sup>a</sup>Correlation of emitter sight-ring and emitting surface temperature from fig. A-1.

TABLE VIII. - Concluded. OUT-OF-PILE TEST DATA AT

ZERO OUTPUT CURRENT

Emitter power input, W	Emitter sight-ring temperature, °C	Emitting surface temperature, °C <sup>a</sup>	Neon pressure		Collector temperature	
			N/m <sup>2</sup>	mm Hg	°C	°F
			333	1235	1190	$1.3 \times 10^2$
410	1300	1245	1.3	1.0	349	660
518	1400	1325	-----	-----	447	836
573	1440	1355	-----	-----	497	927
692	1530	1430	-----	-----	591	1095
765	1575	1465	-----	-----	649	1200
286	1260	1210	$1.3 \times 10^{-1}$	.001	627	1160
312	1260	1210	↓	↓	627	1160
470	1430	1350			746	1375
621	1495 to 1500	1320			788	1450
371	1340	1275			666	1230

<sup>a</sup>Correlation of emitter sight-ring and emitting surface temperature from fig. 17.

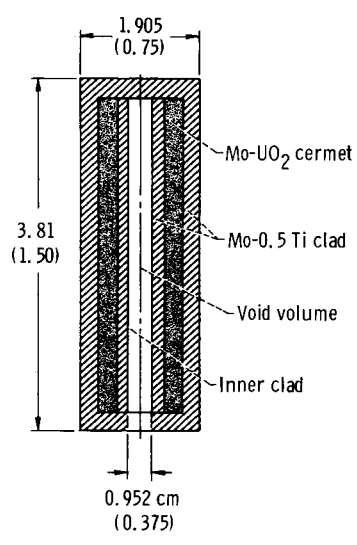
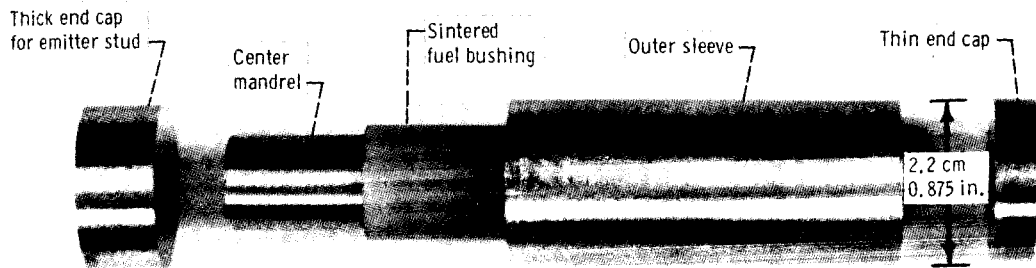
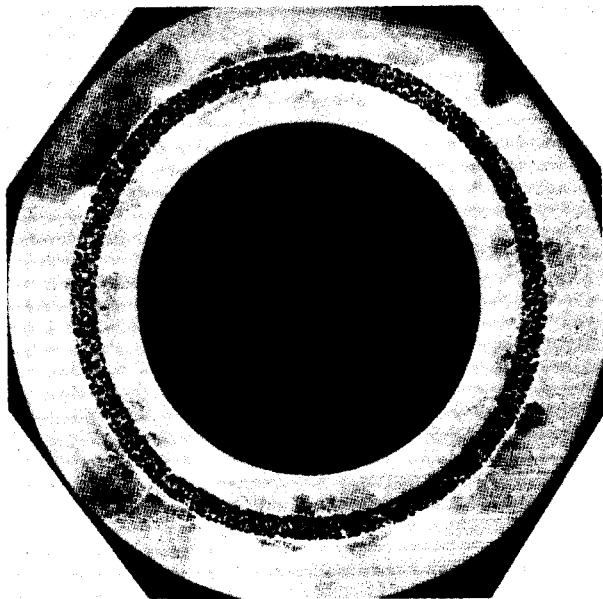


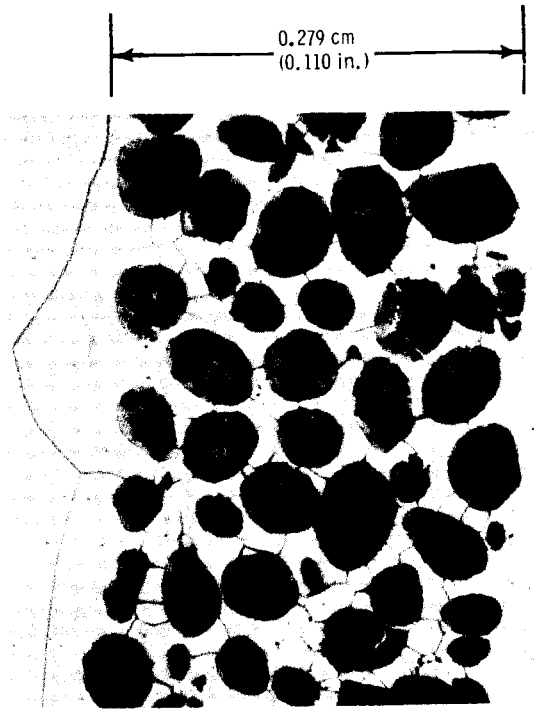
Figure 1. - Experiment fuel form schematic.  
All dimensions are in centimeters (in.).



(a) Exploded view of fuel form.



(b) Photomicrograph of cross-section before final machining, X3.



(c) Photomicrograph of fuel and clad, X100.

Figure 2. - Fuel form.

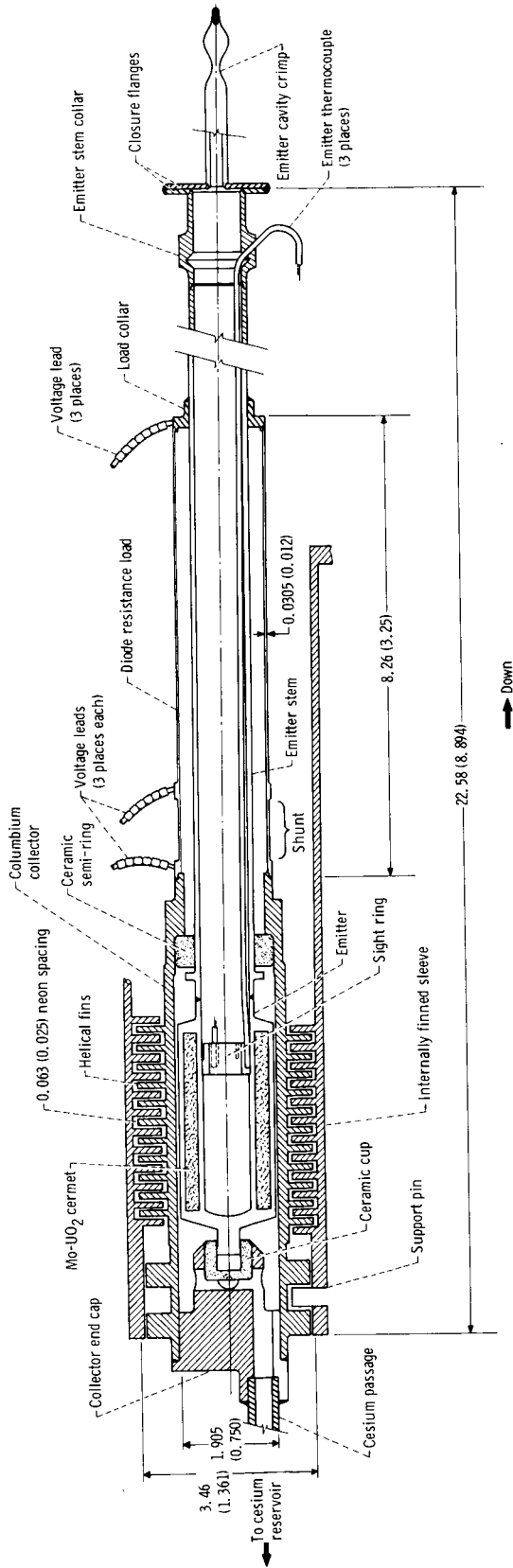


Figure 3. - Diode and load cross section. All dimensions are in centimeters (in.).

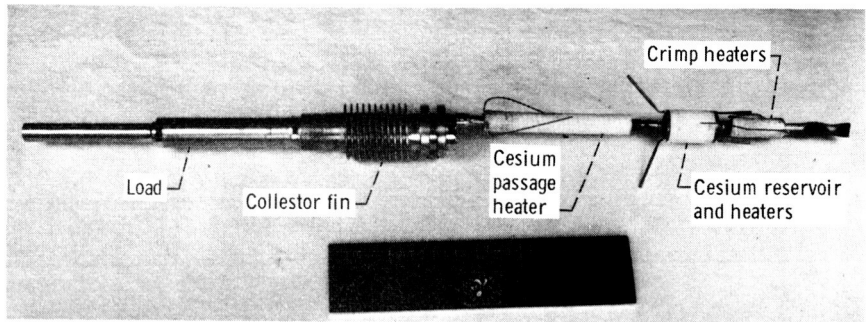


Figure 4. - Cesium-filled diode ready for instrumenting.



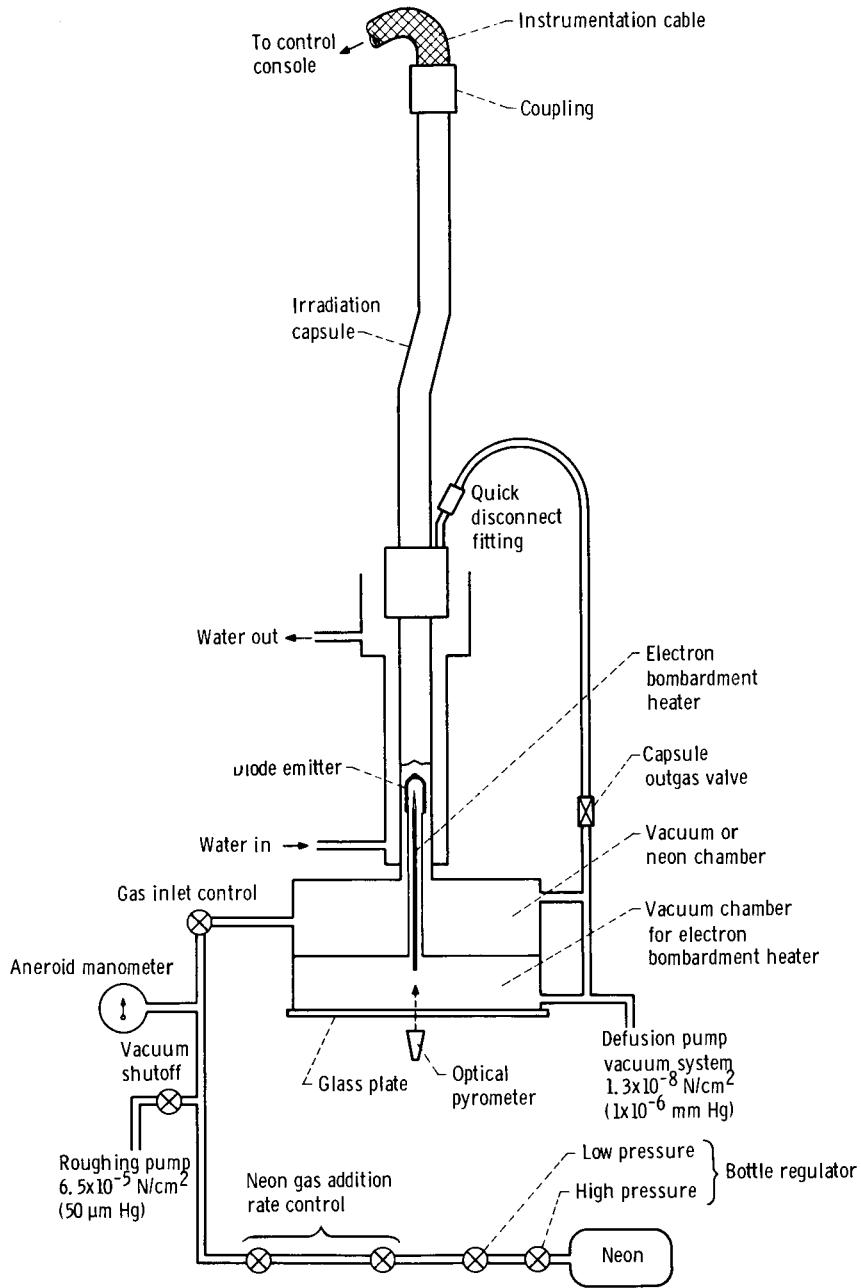


Figure 6. - Schematic of out-of-pile test setup.

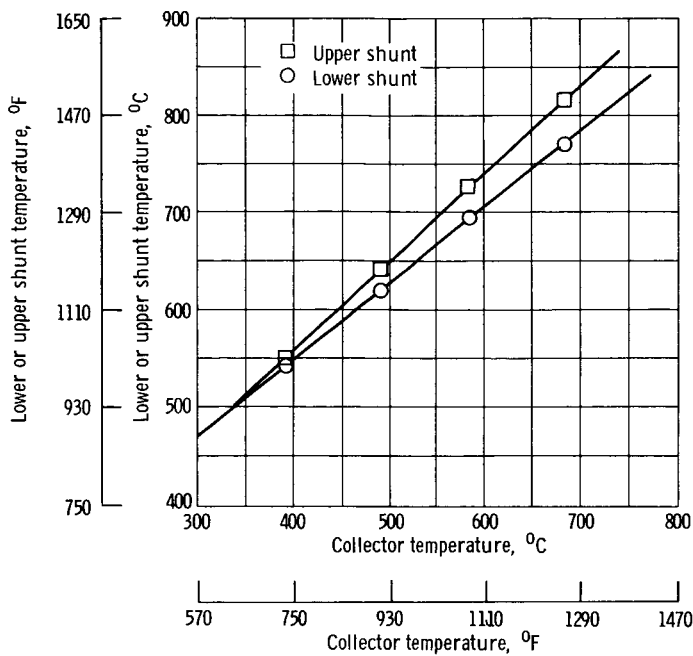


Figure 7. - Collector temperature as function of lower and upper shunt temperature.

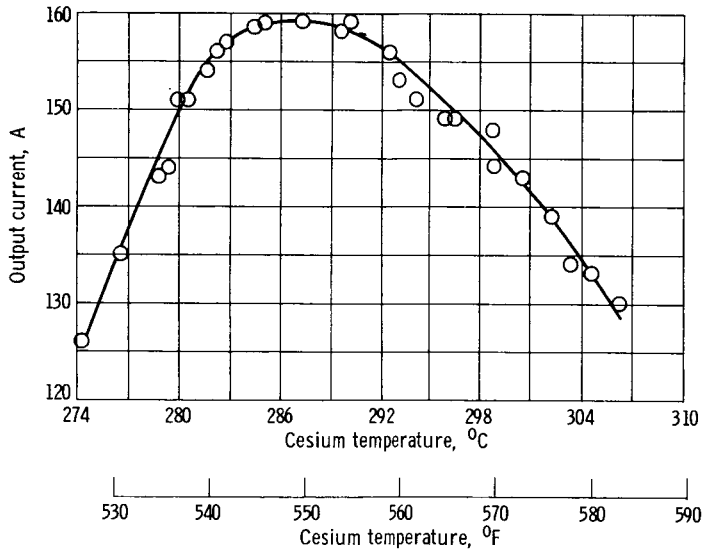


Figure 8. - In-pile data output current as function of cesium temperature for collector temperature of 608° C (1127° F).

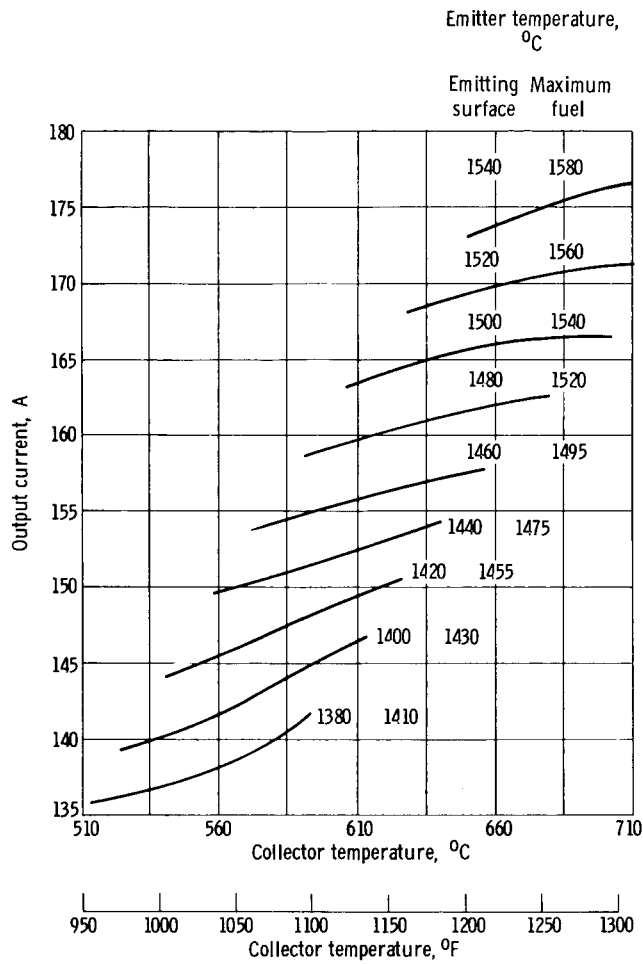
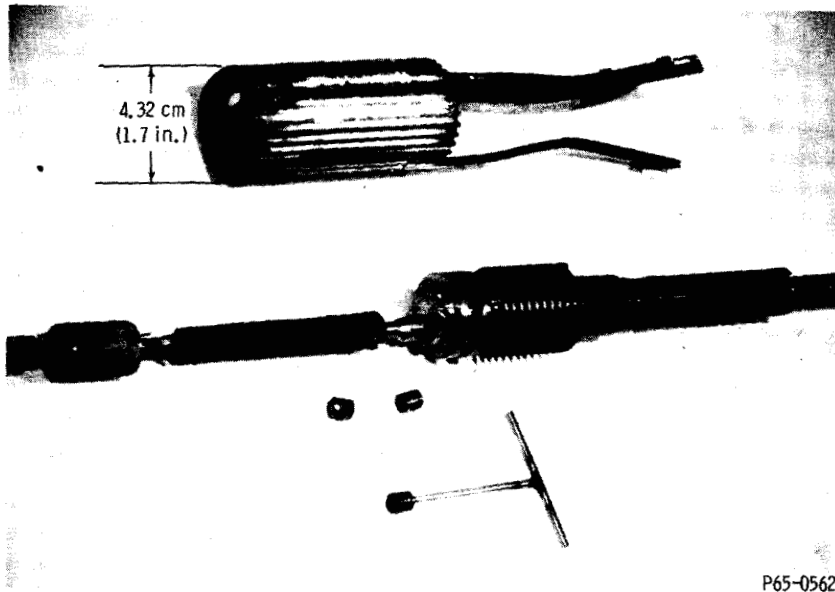


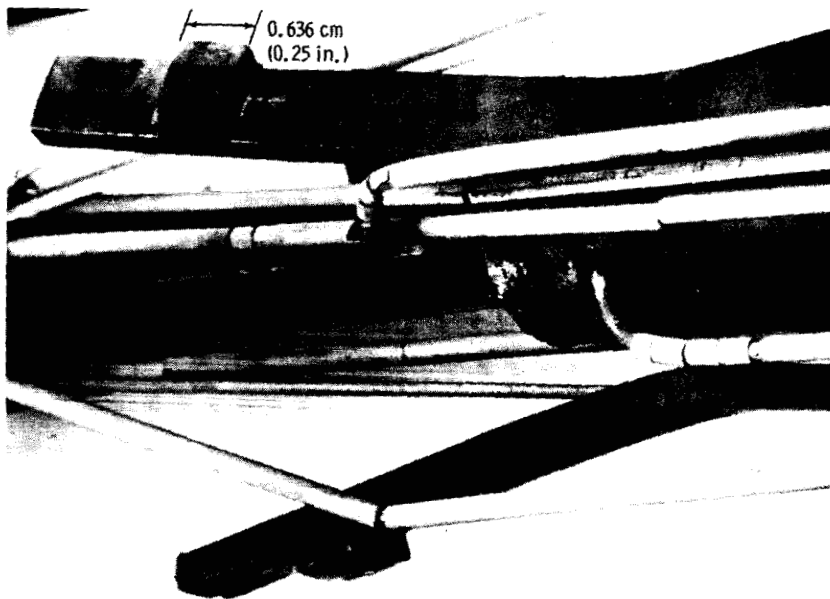
Figure 9. - Out-of-pile performance for maximum output current (at optimum cesium temperature) as function of collector temperature. (See figs. 19 and 24.)

~~CONFIDENTIAL~~



P65-0562

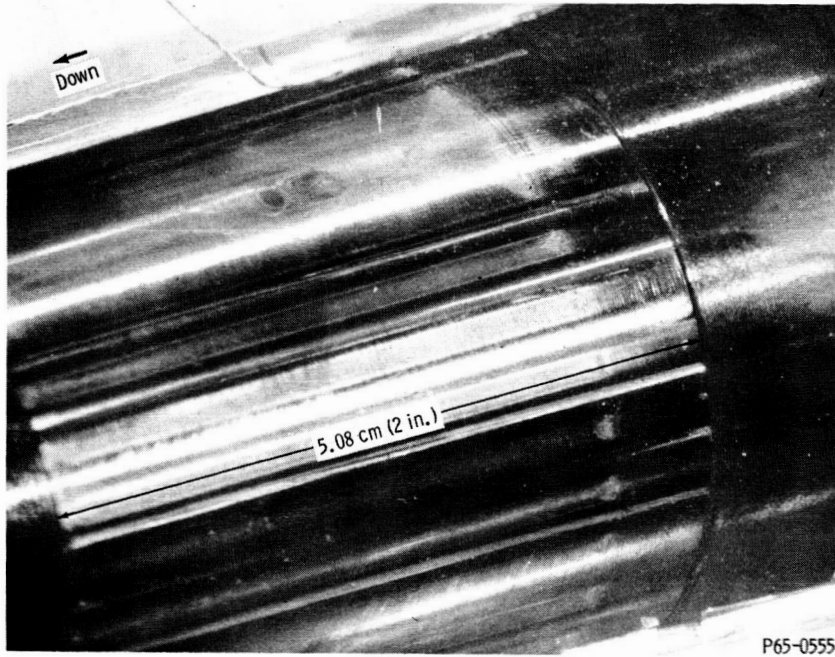
Figure 10. - Bentlegs, diode, and internally finned sleeve after irradiation.



P65-0561

Figure 11. - Bent legs and load area where legs contacted the load.

~~CONFIDENTIAL~~



P65-Q555

Figure 12. - Internally finned sleeve evidence of contact with outer container.

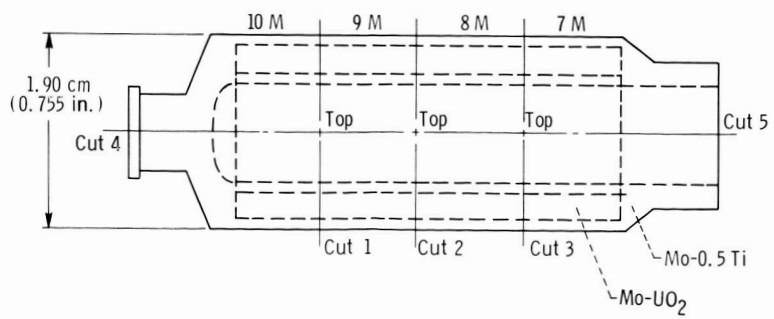


Figure 13. - Emitter sectioning diagram.

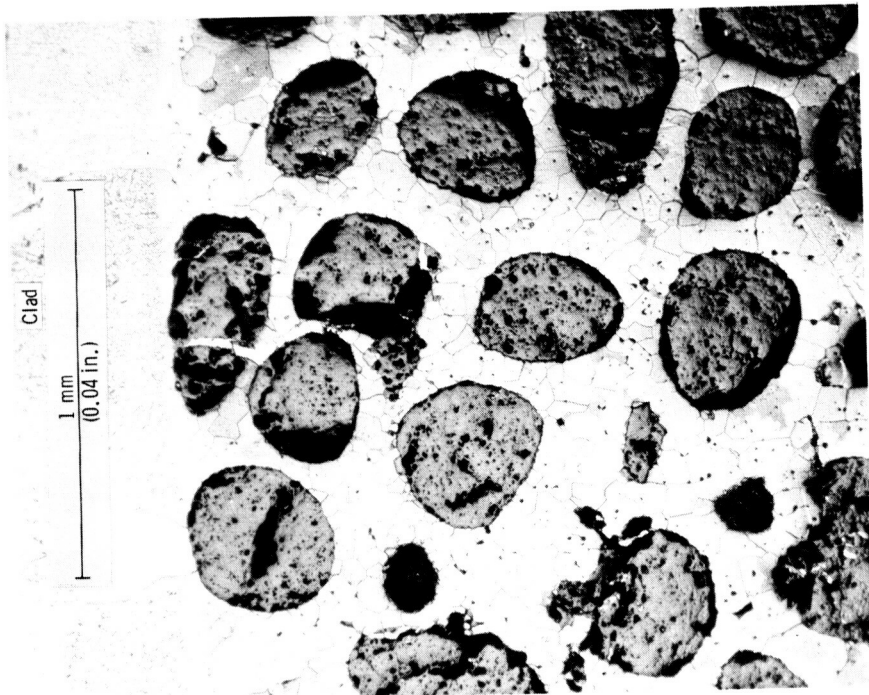


Figure 14. - Photomicrograph showing typical appearance at fuel cermet, clad, and clad to cermet bond. X50.

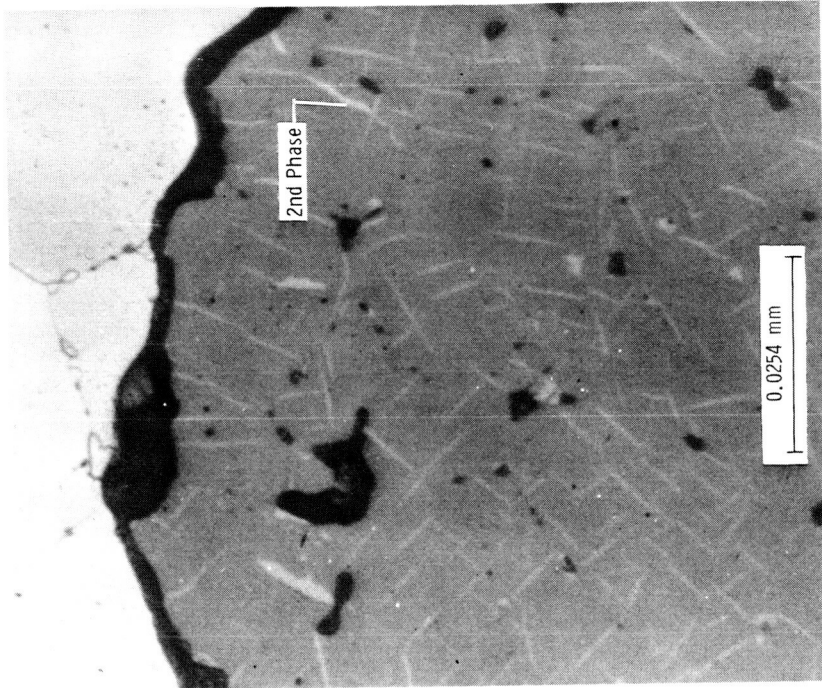
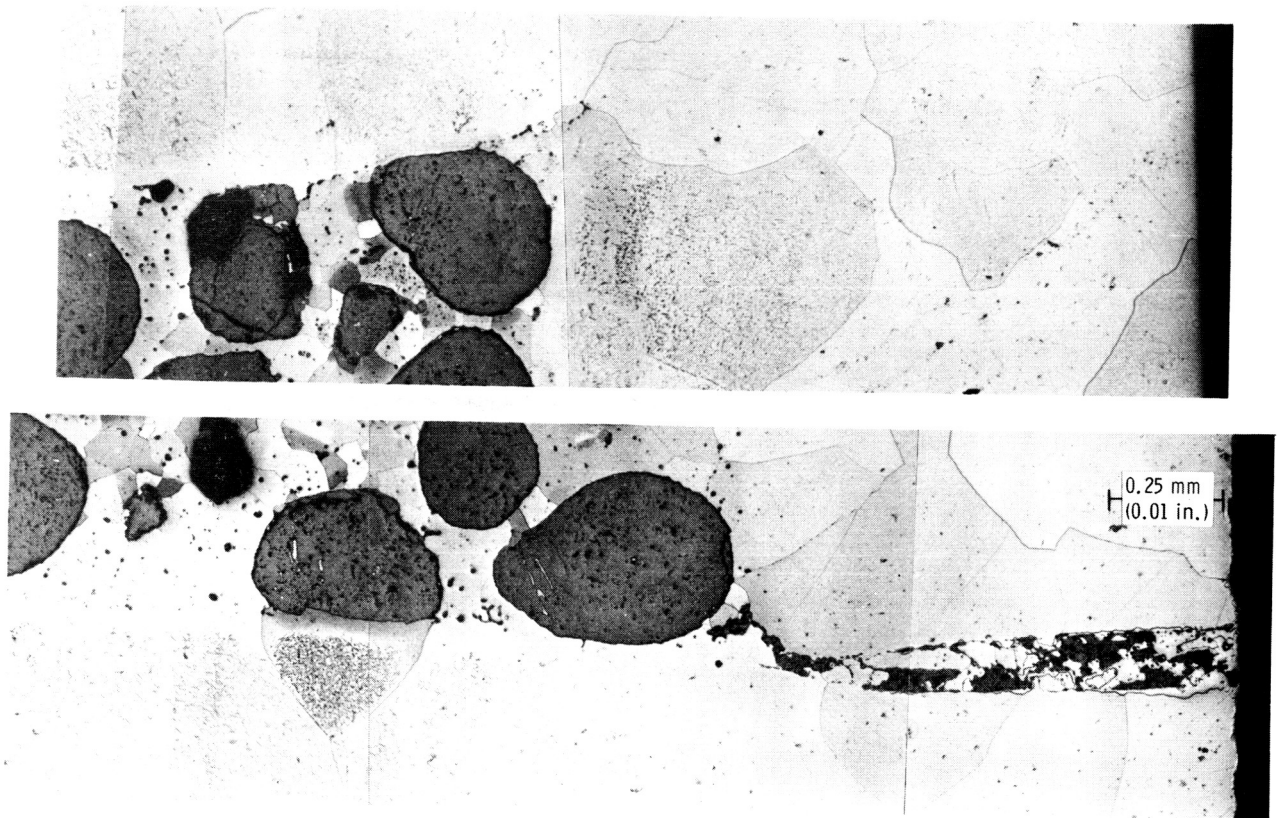


Figure 15. - Photomicrograph of  $UO_2$  particle showing a second phase in  $UO_2$ . X1000.



Failed area

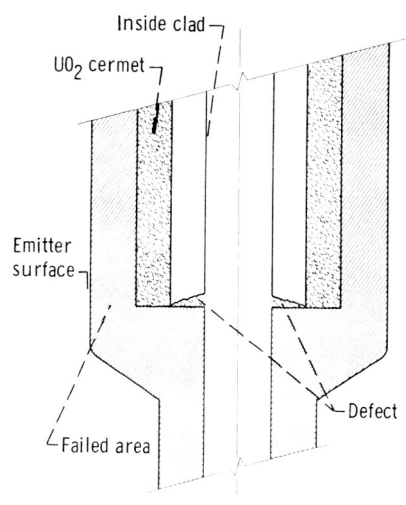


Figure 16. - Montage of photomicrographs through emitter of clad to clad bond line showing cermet fuel extending through inner clad. X100.

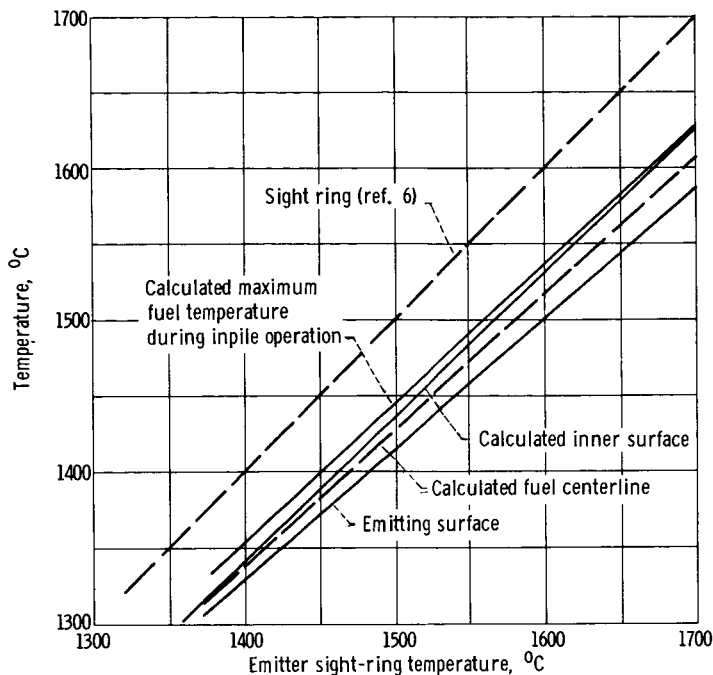


Figure 17. - Correlation of optical sight-ring temperature and emitting surface temperature for TIE-I emitter.

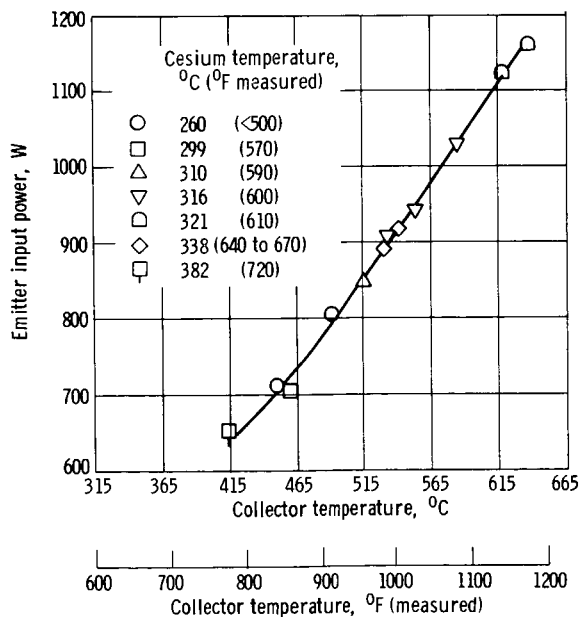


Figure 18. - Emitter input power as function of collector temperature with atmospheric neon. Coolant temperature, 54.4° C (130° F measured).

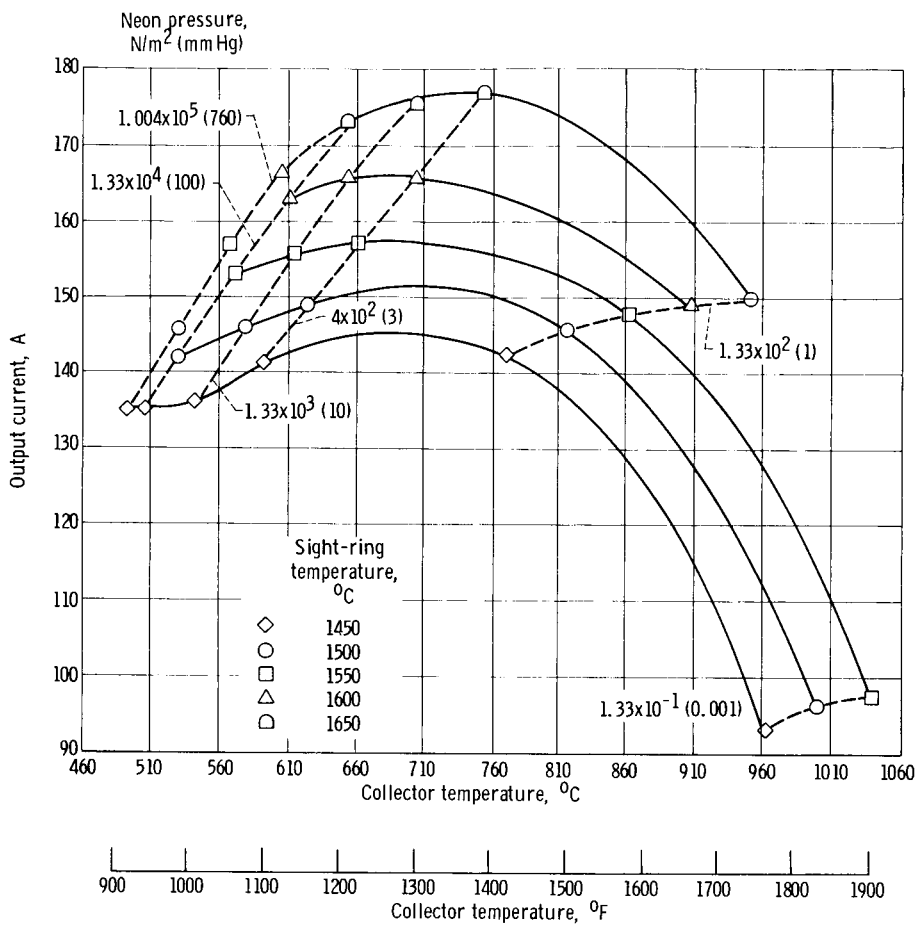


Figure 19. - Output current as function of collector temperature with sight-ring temperature as parameter (optimized cesium temperature).

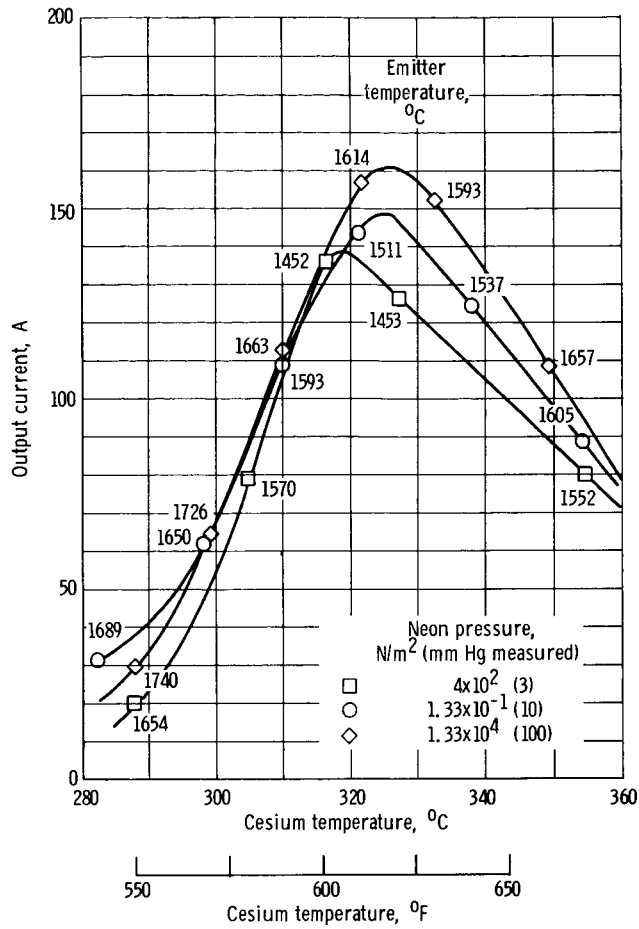


Figure 20. - Output current as function of cesium temperature with neon pressure as parameter at 593° C (1100° F measured) collector temperature.

- R<sub>1</sub> Emitter stem resistance
- R<sub>2</sub> Tantalum load resistance
- E External voltage

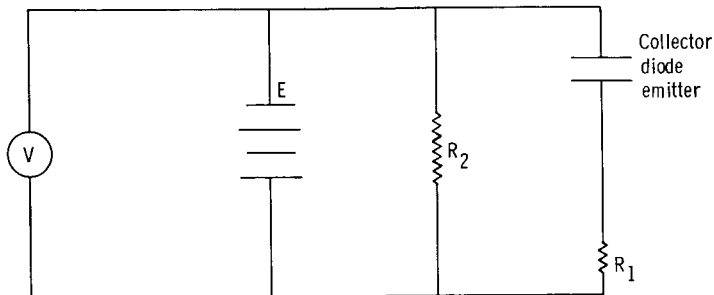


Figure 21. - Diode electrical schematic of diode and loads.

SECRET

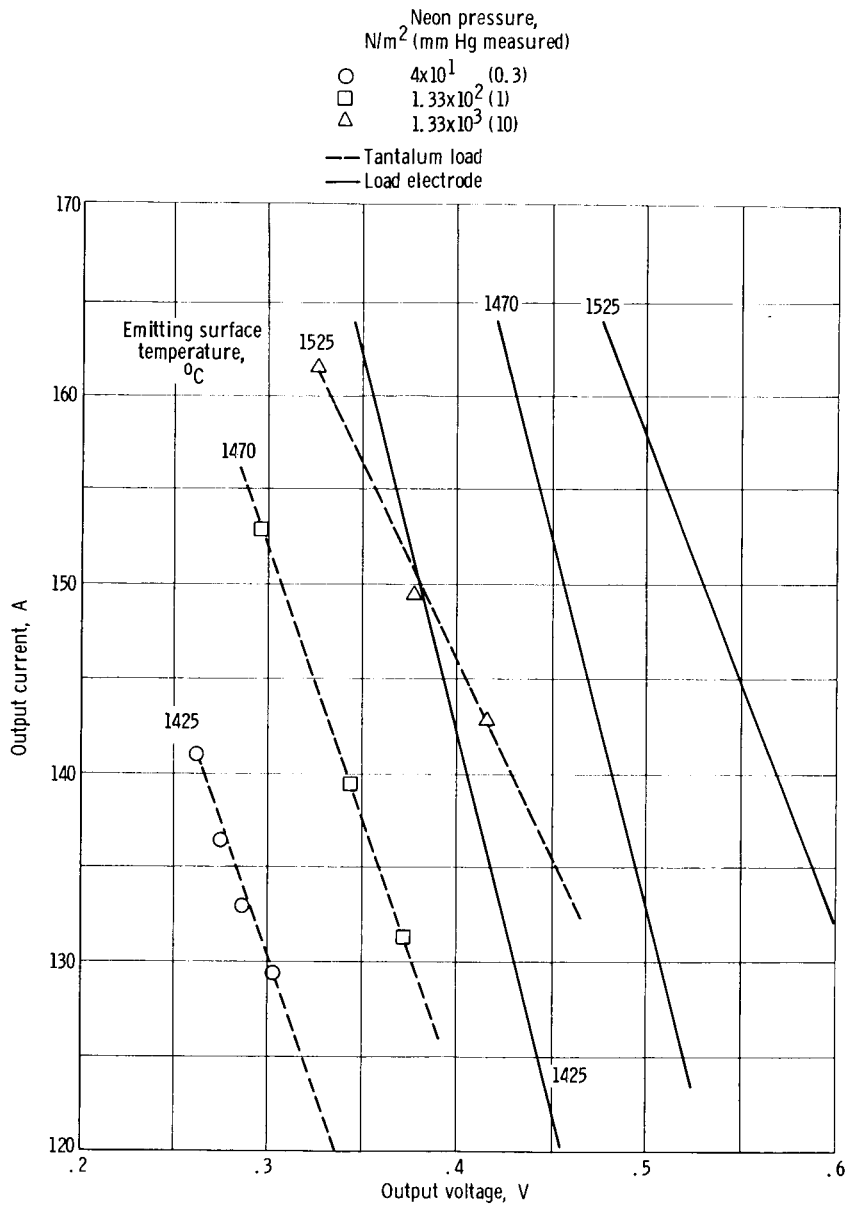


Figure 22. - Current as function of voltage with emitter temperature as parameter (optimized cesium temperature).

SECRET

	Emitting surface temperature, °C	Cesium temperature, °C (°F measured)	Neon pressure, N/m <sup>2</sup> (mm Hg measured)	Collector temperature, °C (°F)
○	1425	362 (683)	4x10 <sup>1</sup> (0.3)	866 (1590)
□	1470	351 (663)	1.3x10 <sup>2</sup> (1.0)	815 (1500)
□	1525	370 (697)	1.3x10 <sup>2</sup> (1.0)	893 (1640)

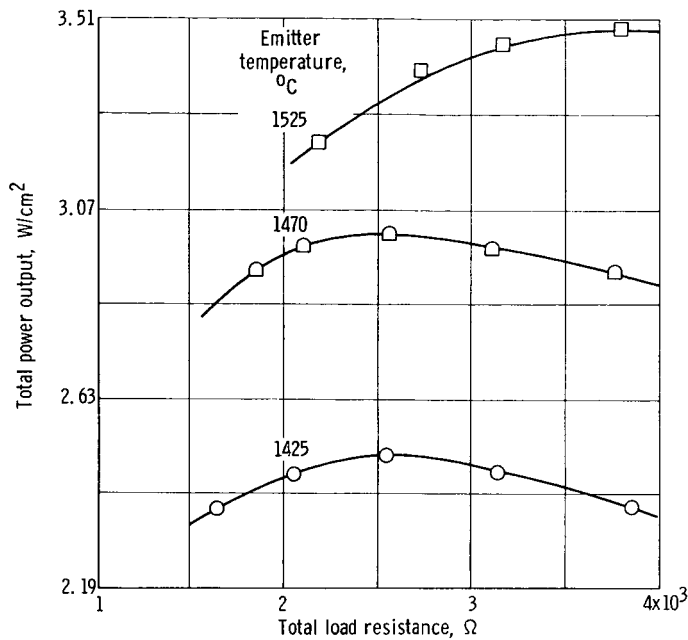


Figure 23. - Total power output as function of total load resistance with emitter temperature as parameter.

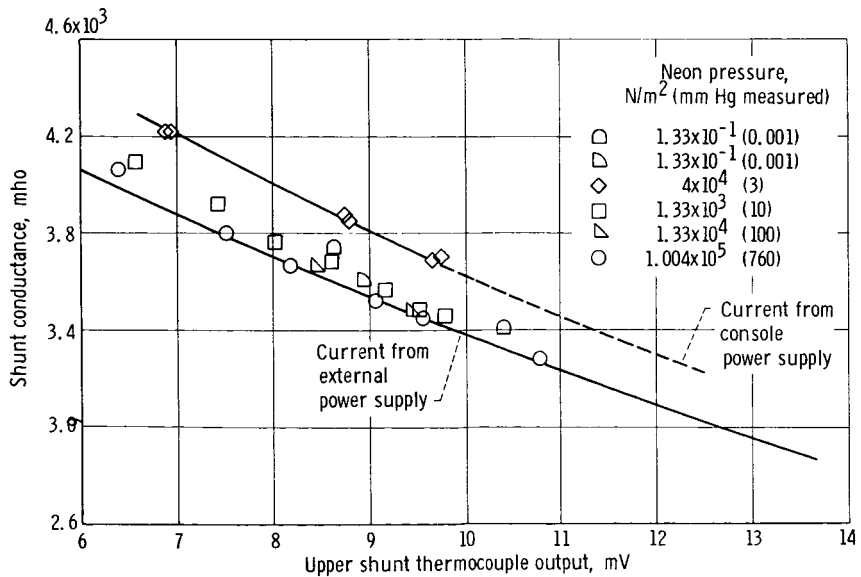


Figure 24. - Shunt calibrations with console and external currents.

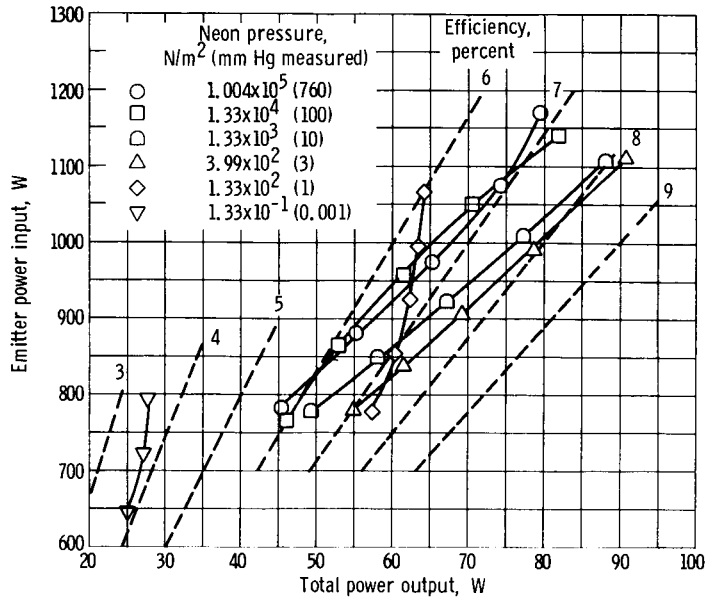


Figure 25. - Emitter power input as function of total power output with neon pressure as parameter (optimized cesium temperature).

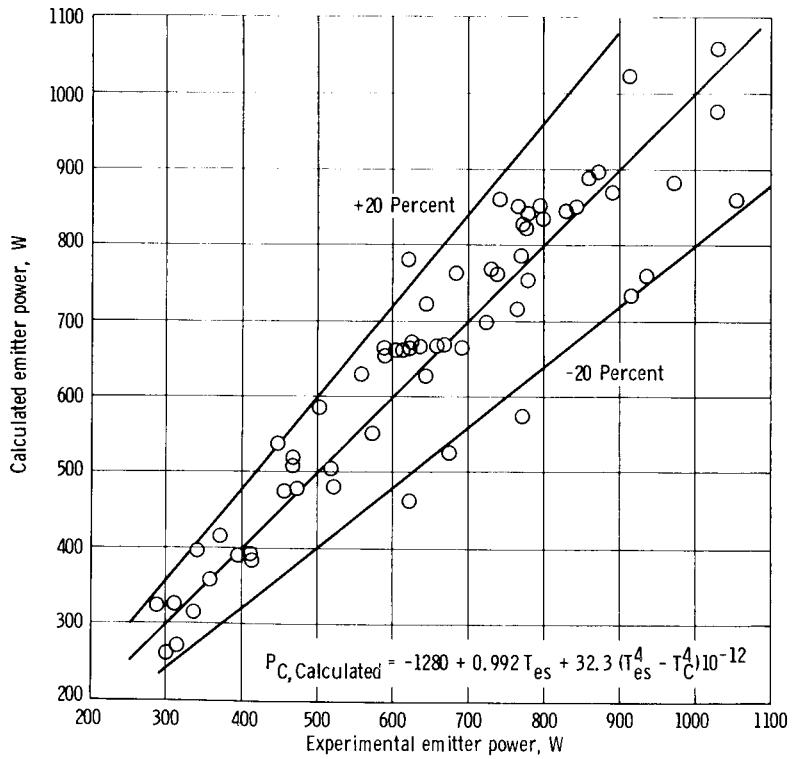


Figure 26. - Least squares fit of zero current emitter power ( $\sigma_{FA}' = 32.3 \times 10^{-12}$  W/K<sup>4</sup> assumed).

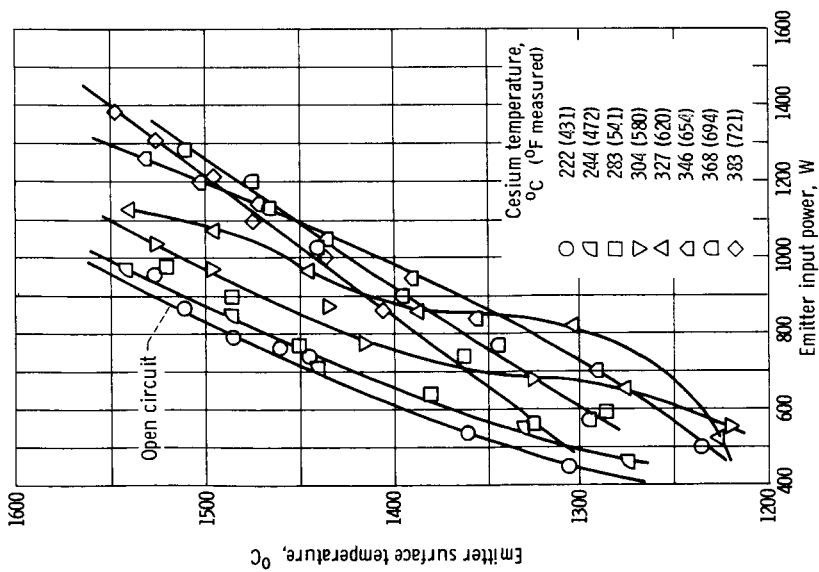


Figure 27. - Emitter temperature as function of emitter power with cesium temperature as parameter. Neon pressure, 39.9 to 53.2 newtons per square meter (0.3 to 0.4 mm Hg measured).

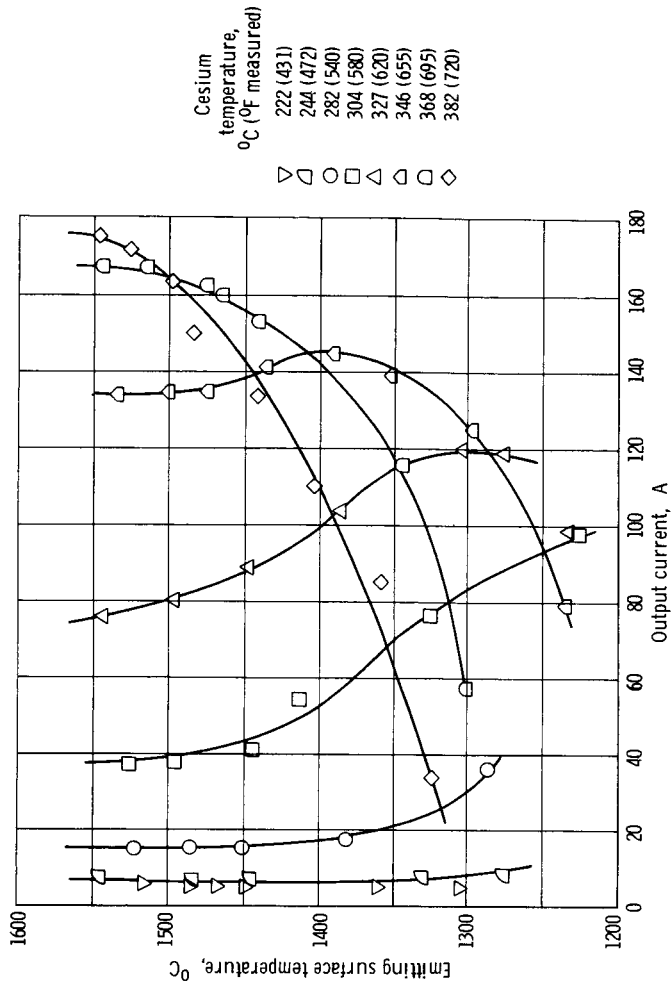


Figure 28. - Emitter temperature as function of output current with cesium temperature as parameter. Neon pressure, 39.9 to 53.2 newtons per square meter (0.3 to 0.4 mm Hg).